Activation of the P2RX7/IL-18 pathway in immune cells attenuates lung fibrosis

Authors

Serena Janho dit Hreich[1,2], Thierry Juhel[1], Sylvie Leroy[2,3,4], Alina Ghinet[5,6,7], Frederic Brau[3], Véronique Hofman[1,2,8,9], Paul Hofman[1,2,8,9], Valérie Vouret-Craviari[1,2]

Affiliations

1. Université Côte d'Azur, CNRS, INSERM, IRCAN, 06108 Nice, France.
2. FHU OncoAge, Nice, France.
3. Université Côte d'Azur, CNRS, Institut Pharmacologie Moléculaire et Cellulaire, Sophia-Antipolis, France.
4. Université Côte d'Azur, Centre Hospitalier Universitaire de Nice, Pneumology Department, Nice, France.
5. Inserm U995, LIRIC, Université de Lille, CHRU de Lille, Faculté de médecine – Pôle recherche, Place Verdun, F-59045 Lille Cedex, France.
6. Hautes Etudes d'Ingénieur (HEI), JUNIA Hauts-de-France, UCLille, Laboratoire de chimie durable et santé, 13 rue de Toul, F-59046 Lille, France.
7. 'Al. I. Cuza' University of Iasi, Faculty of Chemistry, Bd. Carol I, nr. 11, 700506 Iasi, Romania.
8. Laboratory of Clinical and Experimental Pathology and Biobank, Pasteur Hospital, Nice, France.
9. Hospital-Related Biobank (BB-0033-00025), Pasteur Hospital, Nice, France.

Corresponding author: Valérie VOURET-CRAVIARI, IRCAN, 28 Avenue de Valombrose, 06108 Nice, France. Tel 33 (0)492031223. Email : valerie.vouret@univ-cotedazur.fr

Conflict of interest statement: VV-C and AG have a patent related to HEI3090 (PCT/EP2019/058013). All other authors declare they have no competing interests.

Abstract

Idiopathic pulmonary fibrosis (IPF) is an aggressive interstitial lung disease associated with progressive and irreversible deterioration of respiratory functions that lacks curative therapies. Despite IPF being associated with a dysregulated immune response, current antifibrotics aim only at limiting fibroproliferation. We show here that the *P2RX7/IL-18/IFNG* axis is downregulated in IPF patients and that P2RX7 has immunoregulatory functions. Using our positive modulator of P2RX7, we show that activation of the P2RX7/IL-18 axis in immune cells limits lung fibrosis progression in a mouse model by favoring an anti-fibrotic immune environment, with notably an enhanced IL-18-dependent IFN-γ production by lung T cells leading to a decreased production of IL-17 and TGFβ. Overall, we show the ability of the immune system to limit lung fibrosis progression by targeting the immunomodulator P2RX7. Hence, treatment with a small activator of P2RX7 may represent a promising strategy to help patients with lung fibrosis.

Introduction

Idiopathic pulmonary fibrosis (IPF) is an aggressive interstitial lung disease associated with progressive deterioration of respiratory function that is ultimately fatal. It is characterized by destruction of the lung architecture due to accumulation of fibroblasts and extracellular matrix proteins, resulting in increased lung stiffness and impaired normal breathing.

Pirfenidone and nintedanib have been FDA approved for the treatment of IPF since 2014. They target respectively the key fibrotic cytokine TGFβ and several receptor tyrosine kinases, thereby affecting fibroblast activation and extracellular matrix protein production (Heukels et al., 2019). However, they only slow down the progression of the disease, so new therapeutic strategies and targets are needed.

Fibrosis is also associated with inflammation. In fact, fibrosis is a process of excessive wound healing and tissue remodeling due to repeated epithelial injuries releasing damage-associated molecular patterns (DAMPs) that trigger both the adaptive and innate immune systems. Although inflammation has not been considered a target in IPF, due to unsuccessful initial clinical trials of anti-inflammatory drugs (Idiopathic Pulmonary Fibrosis Clinical Research Network et al., 2012) or cyclophosphamide during exacerbations (Naccache et al., 2022), growing evidence suggest that altering specific immune populations that promote or attenuate disease progression may be beneficial (Shenderov et al., 2021).

Extracellular adenosine triphosphate (eATP) is a DAMP, released in high concentrations from injured cells in IPF patients (Riteau et al., 2010). High levels of eATP are recognized by the P2X7 receptor (P2RX7) and P2RX7 participates in the establishment of the bleomycin lung fibrosis mouse model (Riteau et al., 2010). Extracellular activation of P2RX7 by ATP (Surprenant et al., 1996) leads to conformational rearrangements allowing influx of Ca2+ and Na+ ions into and the efflux of K+ ions from the cell (Karasawa et al., 2017) and to the formation of a large pore mediating macrophage cell death. The nature of this large pore was

subjected to controverse until the recent discovery that the macropore function is intrinsic to P2RX7 and does not involve progressive pore dilatation (Harkat et al., 2017; Pippel et al., 2017). Another feature of P2RX7 is its ability to activate the NLRP3 inflammasome, an event linked to potassium efflux (Di et al., 2018; Muñoz-Planillo et al., 2013), which requires both P2RX7 and TWIK2 activation(Di et al., 2018) and leads to the release of mature IL-1β and IL-18 (Perregaux et al., 2000), through gasdermin D pores. Consequently, P2RX7 has the ability to trigger an immune response (Janho Dit Hreich et al., 2023).

IL-1β is a proinflammatory cytokine with high profibrotic properties, as it promotes collagen deposition through IL-17A and TGFβ production (Doerner and Zuraw, 2009; Sutton et al., 2009; Wilson et al., 2010) but also promotes the activation and recruitment of inflammatory cells such as eosinophils and neutrophils. Indeed, deficiency of IL-1βR or its blockade ameliorate experimental fibrosis (Couillin et al., 2009; Gasse et al., 2009, 2007). In contrast, the role of IL-18 is not clear. Indeed, conflicting experimental studies show that IL-18 could either promote (Zhang et al., 2019) or attenuate (Nakatani-Okuda et al., 2005) fibrosis. However, high levels of IL-18BP, a natural antagonist of IL-18, are associated with reduced overall survival in IPF patients (Nakanishi et al., 2021), suggesting that the activity of IL-18 may be required for improved survival or alternatively that high levels of IL-18 are accompanied by more IL-18BP, which leads to poorer outcomes.

IL-18 was originally described as IFN-γ-inducing factor (IGIF) and therefore boosts IFN-γ production by T cells and NK cells (Okamura et al., 1995). Not only has IFN-γ antiproliferative properties (Elias et al., 1987) but it also inhibits TGFβ activity (Ulloa et al., 1999; Varga et al., 1990) and therefore inhibits fibroblast activation and differentiation into myofibroblasts, alleviates TGFβ-mediated immunosuppression, inhibits extracellular matrix accumulation and collagen production(Duncan and Berman, 1985; Gillery et al., 1992; Gurujeyalakshmi and Giri, 1995; Yuan et al., 1999) and thus promotes an antifibrotic immune microenvironment, making

IFN-γ a cytokine with antifibrotic properties. However, parenteral systemic administration of IFN-γ failed in clinical trials (INSPIRE; NCT 00075998) (King et al., 2009), whereas local administration by inhalation showed promising results (Diaz et al., 2012; Fusiak et al., 2015; Prior and Haslam, 1992; Skaria et al., 2015; Smaldone, 2018).

One way to increase IFN-γ production locally and selectively in the lung would be to alter the phenotype of T cells since the polarization of T lymphocytes has been shown to impact fibroblasts' fate and immune infiltrate (Luzina et al., 2008; Shenderov et al., 2021). Indeed, T cells have been recently shown to selectively kill myofibroblasts through IFN-γ release and limit the progression of lung and liver fibrosis in preclinical models (Sobecki et al., 2022) and set up an immune memory in the long term since IFN-γ-producing tissue resident memory T cells protect against fibrosis progression (Collins et al., 2016), highlighting the importance IFN-γ producing T cells in this disease. Accordingly, $CD4^{+}$-producing IFN-γ T cells are decreased in IPF and correlate with a better prognosis in IPF patients (Giri et al., 1986; Luzina et al., 2008; Xu et al., 2006) .

In light of IL-18's demonstrated capability to modulate the T cell phenotype by eliciting IFN-γ, we have posited a novel therapeutic approach for pulmonary fibrosis. Our proposal involves augmenting local IFN-γ production through targeted intervention in the P2RX7/IL-18 axis. This strategy aims to harness the immunomodulatory potential of this axis, offering a promising avenue for therapeutic intervention in pulmonary fibrosis. To implement this strategy, we utilized HEI3090, a chemical compound developed in our laboratory. HEI3090 has been previously reported to enhance the channel activity and large pore opening of P2RX7 and also to increase IL-18 levels (but not IL-1β) upon activation of the P2RX7/NLRP3 pathway (Douguet et al., 2021).

Results

Expression of P2RX7 and IL-18 activity are downregulated in IPF patients

The canonical release of IL-18 is due to activation of the P2RX7/NLRP3 pathway (Perregaux et al., 2000). Since high levels of eATP are found in IPF patients (Riteau et al., 2010) and P2RX7 is activated by such levels, it was of particular interest to investigate the involvement of P2RX7 in this disease. We used a publicly available dataset of lung homogenates from control and IPF patients and compared the mRNA expression levels of P2RX7 and markers of fibrosis, namely *ACTA2*, *COL1A2*, *COL3A1* and *TGFB3*. We found that the mRNA expression of P2RX7 is downregulated in IPF patients (Figure 1A and B), as well as the components of the NLRP3 inflammasome (Supplemental Figure 1). Since IL-18 is constitutively expressed (Puren et al., 1999), which partly explains the lack of difference between control and IPF patients (Figure 1B), we investigated the signaling pathway downstream of IL-18. IL-18 binds to its receptor IL-18R1 coupled to its adaptor protein IL-18RAP which is required for IL-18 signaling and IFN-γ expression. We showed that *IL-18R1*, *IL-18RAP* and *IFN-γ* (Figure 1B) are downregulated in IPF patients. Knowing that the modulation of the phenotype of T cells is promising in IPF (Shenderov et al., 2021), we checked whether P2RX7 and IL-18 are linked to an immune response in IPF patients using Gene Set Enrichment Analyses. Indeed, we showed that the expression of P2RX7 and IL-18 signaling (IL-18 and IL-18RAP) correlates with the IFN-γ response as well as with immunoregulatory interactions required for changing the phenotype of T cells (Figure 1C, Supplemental Figure 1B). This transcriptomic analysis highlights that the P2RX7/IL-18 signaling pathway is downregulated and suggests that this pathway may be able to modulate the immune response in IPF patients.

HEI3090 inhibits the onset of pulmonary fibrosis in the bleomycin mouse model

Even though transcriptomic changes do not always reflect changes in the proteome these encouraging results led us to hypothesize that activation of the P2RX7/IL-18 axis may restrain

lung fibrosis progression by promoting an antifibrotic immune microenvironment. To test this hypothesis, we enhanced the P2RX7/IL-18 axis in the bleomycin (BLM)-induced lung fibrosis mouse model by using HEI3090, a chemical compound described to stimulate immune cells expressing P2RX7 to generate IL-18 in the presence of eATP (Douguet et al., 2021).

We first tested the antifibrotic potential of HEI3090 on mice having an established fibrosis (Figure 2A). Activation of P2RX7 with HEI3090 in mice 7 days after BLM administration reduced the development of pulmonary fibrosis, as evidenced by less thickening of alveolar walls and free air space (Figure 2B). Fibrosis severity was evaluated using the Ashcroft score. To overcome the heterogeneity of fibrosis within the lobes, we scored the whole surface of the lung, and the result represents the mean of each field (Figure 2C and supplementary Figure 2 A and B). This quantification showed that fibrosis is reduced by 40% in lungs of HEI-treated mice.

As accumulation of fibroblasts/myofibroblasts and extracellular matrix proteins are a hallmark of fibrosis, we also quantified fibroblasts/myofibroblasts and collagen levels in the lungs of vehicle and HEI3090-treated mice using respectively an antibody which is specific to the PDGFRα and by measuring the intensity of Sirius Red-stained collagen fibers under polarized light. We showed that both the percentage of CD140a (PDGFRα) positive cells in non-immune cells subset (Figure 2D) and the collagen fibers were reduced in lungs of HEI3090-treated mice (Figure 2, E and F).

We also tested the ability of HEI3090 to limit lung fibrosis progression when administered during the inflammatory phase of the BLM model (Figure 2G) that mimics the exacerbation episodes in IPF patients (Peng et al., 2013). HEI3090 was also able to inhibit the onset of lung fibrosis in this setting given less damage on lung architecture (Figure 2H), the reduced fibrosis score (Figure 2I). We further evaluated the percentage of fibroblasts/myofibroblasts in non-immune cells subset (Figure 2J). At this shorter time point, we observed less

fibroblasts/myofibroblasts in lungs of WT mice treated with vehicle and the number of CD140a positive cells is decreased in lungs of HEI3090-treated mice. Further, and as for mice with an established fibrosis, HEI3090 reduced the intensity of collagen fibers in lungs of HEI3090-treated mice (Figure 2, K and L). We further verified whether the antifibrotic action of HEI3090 depends on the expression of P2RX7 by inducing lung fibrosis in *p2rx7* knockout (KO) mice. In doing so, we initially observed that P2RX7 plays a role in the development of BLM-induced lung fibrosis. This is illustrated by a decrease of 50% in the Ashcroft score, with a mean value of 1.7 in P2RX7 knockout mice compared to 3 in wild-type mice (Figure 2M and Supplemental Figure 2C). It is important to note that *p2rx7* -/- mice still exhibit signs of lung fibrosis, such as thickening of the alveolar wall and a reduction in free air space, in comparison to naïve mice that received PBS instead of BLM (see Supplemental Figure 2A). This result confirms a previous report indicating that BLM-induced lung fibrosis partially depends on the activation of the P2RX7/pannexin-1 axis, leading to the production of IL-1β in the lung. Additionally, in contrast to the observations in WT mice, HEI3090 failed to attenuate the remaining lung fibrosis in *p2rx7* -/- mice, as measured by the Ashcroft score (Figure 2M), the percentage of lung tissue with fibrotic lesions, or the intensity of collagen fibers (Supplemental Figure 2D). These results show that P2RX7 alone participates in fibrosis and that HEI3090 exerts a specific antifibrotic effect through this receptor (see Supplemental Figure 2C).

HEI3090 shapes immune cell infiltration in the lungs

Given that transcriptomic analysis revealed the immunoregulatory functions of P2RX7 in IPF (Figure 1) and the antifibrotic activity of HEI3090 (Figure 2), we subsequently explored whether HEI3090 had an impact on both the immune landscape of the lung and the production of cytokines. This investigation aimed to elucidate the potential mechanisms underlying the dual antifibrotic effects observed with both P2RX7 deletion and P2RX7 activation by HEI3090.

We show that lung CD3+ T cells were more biased to produce IFN-γ than the profibrotic IL-17A cytokine when mice expressing P2RX7 were treated with HEI3090 (Figure 3A and Supplemental Figure 3A). This biased production of IFN-γ is only seen in CD3+ T cells and not in overall lung immune cells (Supplemental Figure 3B) nor in the subsets of T lymphocytes (Figure 3B, Supplemental Figure 3B) or NK cells (Supplemental Figure 3C). Although levels of CD3+ T cells and T cell subsets were unchanged (Supplemental Figure 3D), including the profibrotic Th17 cells (Figure 3C), IL-17A production by Th17 cells is substantially attenuated after HEI3090 treatment (Figure 3C), consistent with the ability of IFN-γ to inhibit IL-17A production (Laurence et al., 2007). Considering the strong profibrotic properties of TGFβ and its mutual antagonism with IFN-γ (Ishida et al., 2004; Park et al., 2007), we checked whether HEI3090 had an effect on TGFβ levels. Indeed, treatment with HEI3090 reduced TGFβ-producing immune cells in the lung as well as TGFβ production (Figure 3D). Notably, HEI3090 treatment reduced TGFβ production in NK cells but not in T-cell subsets (Supplemental Figure 3F).

Pulmonary fibrosis is also favored and driven by the recruitment of inflammatory cells, mainly from the myeloid lineage. Monocytes are highly inflammatory cells that are recruited to the lung and differentiate into alveolar macrophages, both of which have strong profibrotic properties (Gibbons et al., 2011; McCubbrey et al., 2018; Misharin et al., 2017). We demonstrated that in HEI3090-treated mice, the number of inflammatory monocytes decreased markedly (Figure 3G), whereas the number of alveolar macrophages remained unchanged (Figure 3F), consistent with the prognostic ability of monocyte count in IPF progression (Achaiah et al., 2021; Kreuter et al., 2021; Liu et al., 2019; Scott et al., 2019). We also examined other inflammatory cells with profibrotic properties, such as eosinophils (Morimoto et al., 2018) that are less present in HEI3090-treated lungs (Figure 3G), or PMN levels that remain unchanged by HEI3090 treatment (Supplemental Figure 3D).

We also wondered if the activation of P2RX7 has a systemic effect by analyzing immune changes in mice's spleens. No significant change in cell populations was observed in the spleens of mice (Supplemental Figure 4B) when HEI3090 was administrated in the early phase of the BLM model suggesting a local lung activity of the molecule. However, HEI3090 reactivated a systemic immune response with higher levels of dendritic cells and lymphocytes in the spleens of mice treated during the fibroproliferation phase (Supplemental Figure 4D). These results show the ability of HEI3090 to shape the immune response locally and impact the progression of fibrosis systemically even in the fibroproliferative phase of the BLM model.

Altogether these results demonstrate that HEI3090 promotes an antifibrotic cytokinic profile in lung immune cells and attenuates lung inflammation.

HEI3090 requires the P2RX7/NLRP3/IL-18 pathway in immune cells to inhibit lung fibrosis

We wanted to further investigate the mechanism of action of HEI3090 by identifying the cellular compartment and signaling pathway required for its activity. Since the expression of P2RX7 and the P2RX7-dependent release of IL-18 are mostly associated with immune cells (Ferrari et al., 2006), and since HEI3090 shapes the lung immune landscape (Figure 3), we investigated whether immune cells were required for the antifibrotic effect of HEI3090. To do so, we conducted adoptive transfer experiments wherein immune cells from a donor mouse were intravenously injected one day before BLM administration into an acceptor mouse. The intravenous injection route was chosen as it is a standard method for targeting the lungs, as previously documented (Wei and Zhao, 2014). This approach was previously used with success in our laboratory (Douguet et al., 2021). It is noteworthy that this adoptive transfer approach did not influence the response to HEI3090. This was observed consistently in both *p2rx7* -/- mice and *p2rx7* -/- mice that received splenocytes of the same genetic background. In both

cases, HEI3090 failed to mitigate lung fibrosis, as depicted in Figure 2M and Supplemental Figures 2D and 6A and B. First, we tested whether WT P2RX7-expressing splenocytes infuse into *p2rx7* -/- mice restored the antifibrotic activity of HEI3090. We show that restriction of P2RX7 expression on immune cells restored the antifibrotic effect of HEI3090 based on the architecture of the lung, with lungs of HEI3090-treated mice showing more free airspace and thinner alveolar walls (Figure 4B), as well as an overall lower fibrosis score (Figure 4C) and collagen fiber intensity (Figure 4D) than control lungs. Since it was previously showed that the bleomycin mouse model relies on P2RX7-expressing pulmonary epithelial cells (Riteau et al., 2010), we wanted to validate further the role of P2RX7-expressing immune cells in a mouse model where P2RX7 is expressed by non-immune cells. To do so, we reduced both the expression of P2RX7 and its activity by repeated i.v. administration (days 1, 4, 7 9 and 11) of *p2rx7*$^{-/-}$ splenocytes in WT mice (Supplemental Figure 5). In this setting, HEI3090 was unable to limit the progression of fibrosis. These results highlight the important role of immune cells and rules out a major role of non-immune P2RX7-expressing cells, such as fibroblasts, in the antifibrotic effect of HEI3090.

To test the importance of the NLRP3/IL-18 pathway downstream of P2RX7, we performed an adoptive transfer of *nlrp3*$^{-/-}$ and *il18*$^{-/-}$ splenocytes into *p2rx7*$^{-/-}$ mice, expressing similar levels of P2RX7 as WT splenocytes (Supplemental Figure 6E), but also the same levels of IL-18 and NLRP3 (Supplemental Figure 6F). We also verified in this experimental setting by comparing each experimental groups (treated and non-treated) that the genetic background did not affect lung fibrosis (Supplementary Figure 7). The absence of NLRP3 and IL-18 in P2RX7-expressing immune cells abrogated the ability of HEI3090 to inhibit lung fibrosis because the lung architecture and collagen fibers intensity resembled that of control mice (Figure 4, E-J). Consistent with the requirement of IL-18 for HEI3090's antifibrotic activity, activation of P2RX7 with this molecule in WT mice increased the levels of IL-18 in the sera of these mice

compared to control mice (Figure 4K). Moreover, neutralization of IL-18 abrogated the increase of the IFN-γ/IL-17A ratio by lung T cells (Figure 4L), highlighting furthermore the necessity of IL-18 for the antifibrotic effect of HEI3090.

Not only does the activation of the P2RX7/NLRP3 pathway leads to the release of IL-18, but also induce the release of the pro-inflammatory and pro-fibrotic IL-1β cytokine. However, IL-1β was not involved in the antifibrotic effect of HEI3090 (Supplemental Figure 6C), nor were its levels affected by HEI3090 in WT mice (Supplemental Figure 6D), in contrast to IL-18 levels measured in the same biological sample (Figure 4K).

Overall, we show that the P2RX7/NLRP3/IL-18 axis in immune cells is required to limit lung fibrosis progression, highlighting the efficacy in targeting the immune system in this disease.

Discussion

A major unmet need in the field of IPF is new treatment to fight this uncurable disease. In this preclinical study, we demonstrate the ability of immune cells to limit lung fibrosis progression. Based on the hypothesis that a local activation of a T cell immune response and upregulation of IFN-γ production has antifibrotic proprieties, we used the HEI3090 positive modulator of the purinergic receptor P2RX7, previously developed in our laboratory (Douguet et al., 2021), to demonstrate that activation of the P2RX7/IL-18 pathway attenuates lung fibrosis in the bleomycin mouse model. We have demonstrated that lung fibrosis progression is inhibited by HEI3090 in the fibrotic phase but also in the acute phase of the BLM fibrosis mouse model, i.e. during the period of inflammation. This lung fibrosis mouse model commonly employed in preclinical investigations, has recently been recognized as the optimal model for studying IPF (Jenkins et al., 2017). In this model, the intrapulmonary administration of BLM induces DNA damage in alveolar epithelial type 1 cells, triggering cellular demise and the release of ATP. The extracellular release of ATP from injured cells activates the P2RX7/pannexin 1 axis,

initiating the maturation of IL1β and subsequent induction of inflammation and fibrosis. In line with this, mice lacking P2RX7 exhibited reduced neutrophil counts in their bronchoalveolar fluids and decreased levels of IL1β in their lungs compared to WT mice (Riteau et al., 2010). Based on these findings, Riteau and colleagues postulated that the inhibition of P2RX7 activity may offer a potential strategy for the therapeutic control of fibrosis in lung injury. In the present study we provided strong evidence showing that selective activation of P2RX7 on immune cells, through the use of HEI3090, can dampen inflammation and fibrosis by releasing IL-18. The efficacy of HEI3090 to inhibit lung fibrosis was evaluated histologically on the whole lung's surface by evaluating the severity of fibrosis using three independent approaches applied to the whole lung, the Ashcroft score, quantification of fibroblasts/myofibroblasts (CD140a) and polarized-light microscopy of Sirius Red staining to quantify collagen fibers. All these methods of fibrosis assessment revealed that HEI3090 exerts an inhibitory effect on lung fibrosis, underscoring the necessity for a thorough pre-clinical assessment of HEI3090's mode of action. Notably, HEI3090 functions as an activator, rather than an inhibitor, of P2RX7, further emphasizing the importance of elucidating its intricate mechanisms.

Our study showed that inhibition of fibrosis by HEI3090 was associated with an increased production of IFN-γ by lung T cells that was dependent on an increased release of IL-18. The transcriptional analysis additionally indicated the downregulation of the P2RX7/IL-18/IFN-γ pathway in patients with IPF, where TGFβ levels are high (Khalil et al., 1991). This is consistent with the ability of TGFβ to downregulate IL-18R expression and IL-18-mediated IFN-γ production (Koutoulaki et al., 2010). These results confirm the beneficial effects of enhancing activation of the P2RX7/IL-18/IFN-γ pathway.

P2RX7 is expressed by various immune and non-immune cells, but its expression is the highest in dendritic cells (DCs) and macrophages (Di Virgilio and Vuerich, 2015), from which IL-18 is mainly released to shape the T-cell response (Sáez et al., 2017) and increase T-cell IFN-γ

production (Iwai et al., 2008). Collectively, and consistent with the immunomodulatory properties of P2RX7, these observations suggest that HEI3090 may target P2RX7-expressing antigen-presenting cells to influence the T-cell response, which may explain the selective T-cell increase in IFN-γ in HEI3090-treated mice. Accordingly, we have previously shown that HEI3090 targets the P2RX7/IL-18 axis in DCs to shape the immune response in a lung tumor mouse model (Douguet et al., 2021). Noteworthy, by contrast to parenteral administration of IFN-γ which failed in clinical trial (King et al., 2009), we did not observe any sign of systemic side effect likely because HEI3090 needs ATP to potentiate P2RX7 and ATP is present only in injured tissues.

HEI3090 not only increased IFN-γ production by T cells but it also reshaped the immune and cytokinic composition of the lung. Indeed, lungs of HEI3090-treated mice show a decrease in IL-17A production by Th17 cells and TGFβ production by lung immune cells. Moreover, lung inflammation is dampened after HEI3090 treatment, since the number of inflammatory monocytes and eosinophils decreases. It is not known whether this cytokinic and anti-inflammatory switch is solely due to the IL-17A and TGFβ-suppressive property of IFN-γ (de Bruin et al., 2010; Iwamoto et al., 1993; Penton-Rol et al., 1998), or whether it is a combination with the cell death-inducing property of P2RX7 (Surprenant et al., 1996).

Of note, P2RX7 being known to be pro-inflammatory, through IL-1β-release, our strategy to activate P2RX7 with HEI3090 may be considered as risky. However, in line with our prior in vivo and in vitro investigations (Douguet et al., 2021), HEI3090 failed to augment the release of IL-1β in the serum of mice treated with BLM, despite effectively increasing the release of IL-18. This observation elucidates why HEI3090 is effective in alleviating lung fibrosis. In agreement, previous reports have indicated that ATP stimulation of alveolar macrophages, derived from both IPF and lung cancer patients, led exclusively to an elevation in IL-18 levels (Lasithiotaki et al., 2018, 2016), which was explained by an impaired NLRP3 inflammasome

and a defective autophagy in IPF patients (Patel et al., 2012). Autophagy can be regulated by P2RX7 (de Bruin et al., 2010). Indeed, whereas basal autophagy suppresses NLRP3-inflammasome activation and cytokine secretion, induced-autophagy augments IL-1β secretion (Dupont et al., 2011), therefore ruling out the hypothesis of HEI3090-induced autophagy to control the production of IL-1β. Unlike IL-1β, IL-18 is constitutively expressed in human and mouse immune cells (Puren et al., 1999) but also in non-immune cells such as fibroblasts (Artlett et al., 2011) and lung epithelium (Watanabe et al., 2009) and is both matured and released after NLRP3 activation. Therefore, it is currently not known whether the lack of IL-1β release is due to the different cytokine expression pattern or whether there is IL-1β-specific regulation following an enhanced activation of P2RX7 and additional studies are required to answer this question.

In addition to HEI3090, other molecules have been suggested to be positive modulators of P2RX7 *in vitro* (Stokes et al., 2020). Among them the most described are clemastine and ginsenosides. Clemastine, a first generation anti-histaminic, enhances ATP-induced P2RX7 dependent Ca2+ entry, macropore opening and IL1B production in immune cells (Nörenberg et al., 2011). However, when tested *in vivo* clemastine treatment does not activates P2RX7, indeed it reduces the production of pro inflammatory cytokines and decreases P2RX7 expression in hippocampus (Su et al., 2018). These biological responses correspond to an inhibitory effect on P2RX7. Ginsenosides, purified from root of Panax ginseng, have been shown to potentiate ATP-induced P2RX7 dependent Ca2+ entry and macropore opening but also cell death *in vitro* (Helliwell et al., 2015). So far, there is no evidence indicating that ginsenosides act as positive modulators of P2RX7 *in vivo* and all the other chemical compounds described to be active *in vivo* are negative allosteric modulator of P2RX7 (Karasawa and Kawate, 2016).

The novelty of our approach is that it targets and alters the immune environment of the lung. Indeed, the use of a P2RX7-specific modulator that acts only in an ATP-rich environment was effective in promoting an anti-inflammatory and anti-fibrotic phenotype by altering several key mediators of the disease. Therapies given to IPF patients are known to induce significant side effects which can limit their prescription (Raghu et al., 2015). Since current therapies (pirfenidone or nintedanib) and HEI3090 have different mechanisms of action, it could be interesting to test in preclinical studies the efficacy of a treatment combining lower doses of current molecules and HEI3090. If successful, this may open a new therapeutic option to be tested in IPF patients.

In this study, we emphasize the importance of IL-18 for an antifibrotic effect. Several studies have indicated that P2RX7/NLRP3/IL-18 promote disease progression using knock out mice or inhibitors (Artlett et al., 2011; Riteau et al., 2010; Zhang et al., 2019). However, experimental mouse models rely on lung epithelial cell injury that has been shown to activate the NLRP3 inflammasome in the lung epithelium as a first step (Gasse et al., 2009; Riteau et al., 2010) and release danger signals that activate the immune system as a second step. Therefore, initial lung injury to epithelial cells is reduced or absent in *p2rx7*$^{-/-}$ and *nlrp3*$^{-/-}$ mice, indicating that P2RX7 and NLRP3 are required for the establishment of the bleomycin mouse model rather than their role in an already established fibrosis, which has not yet been studied. In addition, NLRP3 and the release of IL-1β and IL-18 from fibroblasts have been shown to promote myofibroblast differentiation and extracellular matrix production (Artlett et al., 2011; Pinar et al., 2020; Watanabe et al., 2009). These observations suggest that fibrosis mouse models initially rely on NLRP3 activation by nonimmune cells and encourage further studies on the contribution of the NLRP3 inflammasome in immune cells to fibrosis progression *in vivo*. Since we have highlighted the importance of this pathway in immune cells for delaying fibrosis progression, we propose that IL-18 may have different effects depending on the cell type. This hypothesis

could be substantiated through experimentation utilizing inducible NLRP3 and P2RX7 knockout mice, wherein the invalidation of NLRP3 and P2RX7 would be induced after the establishment of fibrosis.

Beside an urgent need of new treatments for IPF, there is also a lack of biomarkers, such as prognostic biomarkers, markers of disease activity, or markers of drug efficacy. Our results suggest the possible benefit of an active IL-18 in the pathophysiology of pulmonary fibrosis and warrant analysis of IL-18 as a promising biomarker for predicting outcome in IPF patients. Given the potential effects of pirfenidone and nintedanib on IL-18 levels in preclinical models (Mavrogiannis et al., 2022; Oku et al., 2008; Sharawy and Serrya, 2020), determining IL-18 shifts during treatment would be highly interesting to evaluate potential changes in patients' outcome and to examine IL-18 levels which may be helpful in the long run for patient treatment strategy and subsequent introduction of pipeline drugs (Spagnolo et al., 2021).

Overall, we highlight in this study the ability of the P2RX7/NLRP3/IL-18 pathway in immune cells to inhibit the onset of lung fibrosis by using a positive modulator of P2RX7 that acts selectively in an eATP-rich environment such as fibrotic lung. The unique feature of this strategy is that it enhances the antifibrotic and it attenuates the pro-fibrotic properties of immune cells, with no reported side effects, at least in mice.

Methods

Data availability

In silico data used in this study were retrieved from Gene Expression Omnibus (GEO). We used the Gene expression profiling of "chronic lung disease for the Lung Genomics Research Consortium cohort" (GSE47460, GPL14550). 122 patients with usual Interstitial Pneumonitis (UIP)/ Idiopathic Pulmonary Fibrosis (IPF) and 91 healthy controls were analyzed in this study. Microarray was done on whole lung homogenate from these subjects. Expression profile belong to the Lung Tissue Research Consortium (LTRC).

Mice

Mice were housed under standardized light–dark cycles in a temperature-controlled air-conditioned environment under specific pathogen-free conditions at IRCAN, Nice, France, with free access to food and water. All mouse studies were approved by the committee for Research and Ethics of the local authorities (CIEPAL #598, protocol number APAFIS 21052-2019060610506376) and followed the European directive 2010/63/UE, in agreement with the ARRIVE guidelines. Experiments were performed in accord with animal protection representative at IRCAN. *p2rx7*$^{-/-}$ (B6.129P2-P2rx7tm1Gab/J, from the Jackson Laboratory) were backcrossed with C57BL/6J OlaHsD mice. C57BL/6J OlaHsD male mice (WT) were supplied from Envigo (Gannat, France). The determination of experimental group sizes involved conducting a pilot experiment with four mice in each group. Subsequently, a power analysis, based on the pilot experiment's findings (which revealed a 40% difference with a standard error of 0.9, α risk of 0.05, and power of 0.8), was performed to ascertain the appropriate group size for studying the effects of HEI3090 on BLM-induced lung fibrosis. The results of the pilot experiment and power analysis indicated that a group size of four mice was sufficient to characterize the observed effects. For each full-scale experiment, we initiated the study with 6 to 8 mice per group, ensuring a minimum of 5 mice in each group for robust

statistical analysis. Additionally, we systematically employed the ROULT method to identify and subsequently exclude any outliers present in each experiment before conducting statistical analyses.

Induction of lung fibrosis

WT or *p2rx7*$^{-/-}$ male mice (8 weeks) were anesthetized with ketamine (25mg/kg) and xylazine (2.5 mg/kg) under light isoflurane and were given 2.5 U/kg of bleomycin sulfate (Sigma-Aldrich) by intranasal route. Mice were treated i.p. every day with vehicle (PBS, 10% DMSO) or with HEI3090 (1.5 mg/kg in PBS, 10% DMSO) starting D1 or D7 post bleomycin delivery, as mentioned in the figures. After 14 days of treatment, lungs were either fixed for paraffin embedding or weighted and analyzed by flow cytometry. When mentioned, 200 µg of anti-IL-18 neutralizing antibody (BioXcell) or isotype control (IgG2a, BioXcell) were given by i.p. every three days starting one day prior to BLM administration.

Adoptive transfer in *p2rx7* deficient mice

Spleens from C57BL/6J male mice (8-10 weeks) were collected and digested with the spleen dissociation kit (Miltenyi Biotech) according to the supplier's instructions. 3.10^6 splenocytes were injected i.v. in *p2rx7*$^{-/-}$ mice 1 day before intranasal delivery of bleomycin or when indicated in repeated administration. Mice were treated i.p. every day for 14 days with vehicle (PBS, 10% DMSO) or with HEI3090 (1.5 mg/kg in PBS, 10% DMSO). *Nlrp3*$^{-/-}$ spleens were a kind gift from Dr Laurent Boyer, *il18*$^{-/-}$ spleens from Dr George Birchenough and *il1b*$^{-/-}$ spleens from Dr Bernhard Ryffel, all on a C57BL/6J background.

Histology

Lungs were collected and fixed in 3% formamide for 16 h prior inclusion in paraffin. Deparaffinized lungs sections (3 µm) were rehydrated and sequentially incubated with Hematoxylin, Mayer's, Bluing Reagent and Eosin Y Solution as indicated by the manufacturer

(H&E staining, Abcam, ab245880) or Picro Sirius Red Solution followed by Acetic Acid as indicated by the manufacturer (Picro Sirius Red staining, Abcam, ab150681). The severity of fibrosis was assessed on whole lungs using the Ashcroft modified method which assigns 8 grades (0: normal lung, 1: isolated alveolar septa with gentle fibrotic changes, 2: fibrotic changes of alveolar septa with knot-like formation, 3: contiguous fibrotic walls of alveolar septa, 4: single fibrotic masses, 5: confluent fibrotic masses, 6: large contiguous fibrotic masses, 7: air bubbles and 8: fibrous obliteration to quantify lung fibrosis) to reliable and reproducible quantify fibrosis-induced lung remodeling (Hübner et al., 2008). To be even more accurate and not biased by patchy lesions observed in all existing lung fibrosis induced mouse models, the whole lungs (left and right lobes) were divided in section of 880 µm2 and each section was scored individually as shown in Supplementary Figure 2. A total of 80 to 110 sections were analyzed per mouse.

Levels of collagen on whole lungs were assessed on Sirius Red polarized light images of the entire lung taken with HD - Axio Observer Z1 Microscope ZEISS microscope (Figure 2) or with the SLIDEVIEW V200 slide scanner, Evident Europe Rungis (Figure 4). The collagen amount given by the polarization intensity of the Sirius red staining of the lung slices and the percentage of fibrotic area was quantified with an ImageJ/Fiji macro program as following: The mean gray value and the integrated intensity of the collagen staining were measured in the fibrotic and non-fibrotic regions excluding the signal coming from vessels and bronchial tubes using dedicated masks. The binary masks were obtained after a median filtering and a manual thresholding, from the brightfield images for the fibrotic and non-fibrotic ones and the polarization images for the vessels and bronchial tubes. Vessels and bronchial tubes are excluded from fibrotic and non-fibrotic masks by intersecting each of those masks with the vessel and bronchial tubes one. The resulting masks are then also intersected with the polarization image to measure specifically the mean gray value and integrated intensity of

fibrotic and non-fibrotic areas. The percentage of fibrotic area is obtained from the fibrotic and non-fibrotic masks without vessels and bronchial tubes as the ratio between the fibrotic area and the whole lung area without vessels and bronchial tubes (non-fibrotic + fibrotic).

Cells phenotyping by flow cytometry

Lungs or spleens were collected and digested with the lung or spleen dissociation kit (Miltenyi Biotech, ref 130-095-927 and 130-095-928) according to the supplier's instructions. Red blood cells were lysed using ACK lysis buffer (Gibco, A1049201). Fc receptors were blocked using anti-CD16/32 (2.4G2) antibodies followed by surface staining by incubating cells on ice, for 20 min, with saturating concentrations of labeled Abs (Table 1) in PBS, 5% FBS and 0.5% EDTA. Tregs were identified using the transcription factor staining Buffer Set (eBioscience) for FoxP3 staining. Intracellular staining was performed after stimulation of single-cell suspensions with Phorbol 12- myristate 13-acetate (PMA at 50 ng mL−1, Sigma), ionomycin (0.5 μg mL−1, Sigma) and 1 μL mL−1 Golgi Plug™ (BD Biosciences) for 4 h at 37°C 5% CO2. Cells were then incubated with Live/Dead stain (Invitrogen), according to the manufacturer protocol prior to surface staining. Fc receptors were blocked using anti-CD16/32 (2.4G2) antibodies followed by surface staining by incubating cells on ice, for 20 min, with saturating concentrations of labeled Abs (Table 1) in PBS, 5% FBS and 0.5% EDTA. Cytofix/Cytoperm™ kit (BD biosciences) was used for intracellular stainings by following the manufacturer's instructions. Samples were acquired on CytoFLEX LX (Beckman Coulter) and analyzed using FlowJo (LLC).

ELISA

Sera of mice were collected at the end of the experiment and stored at −80 °C before cytokine detection by ELISA using mouse IL-1 beta/IL-1F2 (R&D, DY401) and IL-18 (MBL, ref 7625) according to the supplier's instructions.

Western Blot

Single cell suspensions of whole lungs were lysed with Laemmli buffer (10% glycerol, 3% SDS, 10 mM Na2HPO4) with protease inhibitor cocktail (Roche). Proteins were separated on a 12% SDS-PAGE gel and electro transferred onto PVDF membranes, which were blocked for 30 min at RT with 3% bovine serum albumin or 5% milk. Membranes were incubated with primary antibodies (see Table 1) diluted at 4 °C overnight. Secondary antibodies (Promega) were incubated for 1 h at RT. Immunoblot detection was achieved by exposure with a chemiluminescence imaging system (PXI Syngene, Ozyme) after membrane incubation with ECL (Immobilon Western, Millipore). The bands intensity values were normalized to that of β-actin using ImageJ software.

Statistical analyses

Quantitative data were described and presented graphically as medians and interquartiles or means and standard deviations. The distribution normality was tested with the Shapiro's test and homoscedasticity with a Bartlett's test. For two categories, statistical comparisons were performed using the Student's t-test or the Mann–Whitney's test. For three and more categories, analysis of variance (ANOVA) or non-parametric data with Kruskal–Wallis was performed to test variables expressed as categories versus continuous variables. If this test was significant, we used the Tukey's test to compare these categories and the Bonferroni's test to adjust the significant threshold. For the Gene Set Enrichment Analyses (GSEA), bilateral Kolmogorov–Smirnov test, and false discovery rate (FDR) were used.

All statistical analyses were performed by biostatistician using Prism8 program from GraphPad software. Tests of significance was two-tailed and considered significant with an alpha level of $P < 0.05$. (graphically: * for $P < 0.05$, ** for $P < 0.01$, *** for $P < 0.001$).

Data and materials availability: All data are available in the main text or the supplementary materials. RNAseq data from IPF and control patients were retrieved from GEO database under the accession number (GSE47460, GPL14550).

Author contributions:

Conceptualization and design: SJH, VV-C

Methodology: SJH, FB

Investigation: SJH, TJ, VV-C

Analysis and Interpretation: SJH, SL, PH, VH, VV-C

Reagents: AG

Writing: SJH, VV-C

Acknowledgments

The authors wish to thank Dr George Birchenough, Dr Laurent Boyer and Dr Bernhard Ryffel for sharing *il18*$^{-/-}$, *nlrp3*$^{-/-}$ and *il1b*$^{-/-}$ spleens respectively. We thank the MICA platform labeled by IBISA and EVIDENT Europe for their help with image analysis. We are grateful to Anna Zelena, EVIDENT Technology Center Europe GmbH, and Fabien Bertholle, EVIDENT Europe GmbH - French Branch, who gave us access to their slide scanner. We acknowledge Clement Molina for his help with the *in vivo* experiments during the revision of the paper. This publication is based upon discussion from PRESTO COST action CA21130 supported by COST (European Cooperation in Science and Technology).

Funding: Ligue Nationale Contre le Cancer (SJH), Fondation pour la recherche médicale grant number #FDT202106013099 (SJH), ARC grant number ARCTHEM2021020003478 (SJH, VV-C), Cancéropôle PACA (VV-C)

The French Government (National Research Agency, ANR through the "Investments for the Future": program reference #ANR-11-LABX-0028-01 (PH), Executive Unit for Financing

Higher Education, Research, Development and Innovation (UEFISCDI), Bucharest, Romania (grant number PN-III-P4-ID-PCE-2020-0818, acronym REPAIR) (AG).

References

Achaiah A, Rathnapala A, Pereira A, Bothwell H, Dwivedi K, Barker R, Benamore R, Hoyles RK, Iotchkova V, Ho L-P. 2021. Monocyte and neutrophil levels are potentially linked to progression to IPF for patients with indeterminate UIP CT pattern. *BMJ open Respir Res* **8**. doi:10.1136/bmjresp-2021-000899

Artlett CM, Sassi-Gaha S, Rieger JL, Boesteanu AC, Feghali-Bostwick CA, Katsikis PD. 2011. The inflammasome activating caspase 1 mediates fibrosis and myofibroblast differentiation in systemic sclerosis. *Arthritis Rheum* **63**:3563–74. doi:10.1002/art.30568

Collins SL, Chan-Li Y, Oh M, Vigeland CL, Limjunyawong N, Mitzner W, Powell JD, Horton MR. 2016. Vaccinia vaccine-based immunotherapy arrests and reverses established pulmonary fibrosis. *JCI insight* **1**:e83116. doi:10.1172/jci.insight.83116

Couillin I, Vasseur V, Charron S, Gasse P, Tavernier M, Guillet J, Lagente V, Fick L, Jacobs M, Coelho FR, Moser R, Ryffel B. 2009. IL-1R1/MyD88 signaling is critical for elastase-induced lung inflammation and emphysema. *J Immunol* **183**:8195–202. doi:10.4049/jimmunol.0803154

de Bruin AM, Buitenhuis M, van der Sluijs KF, van Gisbergen KPJM, Boon L, Nolte MA. 2010. Eosinophil differentiation in the bone marrow is inhibited by T cell-derived IFN-gamma. *Blood* **116**:2559–69. doi:10.1182/blood-2009-12-261339

Di A, Xiong S, Ye Z, Malireddi RKS, Kometani S, Zhong M, Mittal M, Hong Z, Kanneganti T-D, Rehman J, Malik AB. 2018. The TWIK2 Potassium Efflux Channel in Macrophages Mediates NLRP3 Inflammasome-Induced Inflammation. *Immunity* **49**:56-65.e4. doi:10.1016/j.immuni.2018.04.032

Di Virgilio F, Vuerich M. 2015. Purinergic signaling in the immune system. *Auton Neurosci* **191**:117–23. doi:10.1016/j.autneu.2015.04.011

Diaz KT, Skaria S, Harris K, Solomita M, Lau S, Bauer K, Smaldone GC, Condos R. 2012. Delivery and safety of inhaled interferon-γ in idiopathic pulmonary fibrosis. *J Aerosol Med Pulm Drug Deliv* **25**:79–87. doi:10.1089/jamp.2011.0919

Doerner AM, Zuraw BL. 2009. TGF-beta1 induced epithelial to mesenchymal transition (EMT) in human bronchial epithelial cells is enhanced by IL-1beta but not abrogated by corticosteroids. *Respir Res* **10**:100. doi:10.1186/1465-9921-10-100

Douguet L, Janho dit Hreich S, Benzaquen J, Seguin L, Juhel T, Dezitter X, Duranton C, Ryffel B, Kanellopoulos J, Delarasse C, Renault N, Furman C, Homerin G, Féral C, Cherfils-Vicini J, Millet R, Adriouch S, Ghinet A, Hofman P, Vouret-Craviari V. 2021. A small-molecule P2RX7 activator promotes anti-tumor immune responses and sensitizes lung tumor to immunotherapy. *Nat Commun* **12**:653. doi:10.1038/s41467-021-20912-2

Duncan MR, Berman B. 1985. Gamma interferon is the lymphokine and beta interferon the monokine responsible for inhibition of fibroblast collagen production and late but not early fibroblast proliferation. *J Exp Med* **162**:516–27. doi:10.1084/jem.162.2.516

Dupont N, Jiang S, Pilli M, Ornatowski W, Bhattacharya D, Deretic V. 2011. Autophagy-based unconventional secretory pathway for extracellular delivery of IL-1β. *EMBO J* **30**:4701–11. doi:10.1038/emboj.2011.398

Elias JA, Jimenez SA, Freundlich B. 1987. Recombinant gamma, alpha, and beta interferon regulation of human lung fibroblast proliferation. *Am Rev Respir Dis* **135**:62–5. doi:10.1164/arrd.1987.135.1.62

Ferrari D, Pizzirani C, Adinolfi E, Lemoli RM, Curti A, Idzko M, Panther E, Di Virgilio F. 2006. The P2X7 receptor: a key player in IL-1 processing and release. *J Immunol* **176**:3877–83. doi:10.4049/jimmunol.176.7.3877

Fusiak T, Smaldone GC, Condos R. 2015. Pulmonary Fibrosis Treated with Inhaled Interferon-gamma (IFN-γ). *J Aerosol Med Pulm Drug Deliv* **28**:406–10. doi:10.1089/jamp.2015.1221

Gasse P, Mary C, Guenon I, Noulin N, Charron S, Schnyder-Candrian S, Schnyder B, Akira S, Quesniaux VFJ, Lagente V, Ryffel B, Couillin I. 2007. IL-1R1/MyD88 signaling and the inflammasome are essential in pulmonary inflammation and fibrosis in mice. *J Clin Invest* **117**:3786–99. doi:10.1172/JCI32285

Gasse P, Riteau N, Charron S, Girre S, Fick L, Pétrilli V, Tschopp J, Lagente V, Quesniaux VFJ, Ryffel B, Couillin I. 2009. Uric acid is a danger signal activating NALP3 inflammasome in lung injury inflammation and fibrosis. *Am J Respir Crit Care Med* **179**:903–13. doi:10.1164/rccm.200808-1274OC

Gibbons MA, MacKinnon AC, Ramachandran P, Dhaliwal K, Duffin R, Phythian-Adams AT, van Rooijen N, Haslett C, Howie SE, Simpson AJ, Hirani N, Gauldie J, Iredale JP, Sethi T, Forbes SJ. 2011. Ly6Chi monocytes direct alternatively activated profibrotic macrophage regulation of lung fibrosis. *Am J Respir Crit Care Med* **184**:569–81. doi:10.1164/rccm.201010-1719OC

Gillery P, Serpier H, Polette M, Bellon G, Clavel C, Wegrowski Y, Birembaut P, Kalis B, Cariou R, Maquart FX. 1992. Gamma-interferon inhibits extracellular matrix synthesis and remodeling in collagen lattice cultures of normal and scleroderma skin fibroblasts. *Eur J Cell Biol* **57**:244–53.

Giri SN, Hyde DM, Marafino BJ. 1986. Ameliorating effect of murine interferon gamma on bleomycin-induced lung collagen fibrosis in mice. *Biochem Med Metab Biol* **36**:194–7. doi:10.1016/0885-4505(86)90124-6

Gurujeyalakshmi G, Giri SN. 1995. Molecular mechanisms of antifibrotic effect of interferon gamma in bleomycin-mouse model of lung fibrosis: downregulation of TGF-beta and procollagen I and III gene expression. *Exp Lung Res* **21**:791–808. doi:10.3109/01902149509050842

Harkat M, Peverini L, Cerdan AH, Dunning K, Beudez J, Martz A, Calimet N, Specht A, Cecchini M, Chataigneau T, Grutter T. 2017. On the permeation of large organic cations through the pore of ATP-gated P2X receptors. *Proc Natl Acad Sci U S A* **114**:E3786–E3795. doi:10.1073/pnas.1701379114

Helliwell RM, ShioukHuey CO, Dhuna K, Molero JC, Ye J, Xue CC, Stokes L. 2015. Selected ginsenosides of the protopanaxdiol series are novel positive allosteric modulators of <scp>P</scp> 2 <scp>X</scp> 7 receptors. *Br J Pharmacol* **172**:3326–3340. doi:10.1111/bph.13123

Heukels P, Moor CC, von der Thüsen JH, Wijsenbeek MS, Kool M. 2019. Inflammation and immunity in IPF pathogenesis and treatment. *Respir Med* **147**:79–91. doi:10.1016/j.rmed.2018.12.015

Hübner R-H, Gitter W, El Mokhtari NE, Mathiak M, Both M, Bolte H, Freitag-Wolf S, Bewig B. 2008. Standardized quantification of pulmonary fibrosis in histological samples. *Biotechniques* **44**:507–11, 514–7. doi:10.2144/000112729

Idiopathic Pulmonary Fibrosis Clinical Research Network, Raghu G, Anstrom KJ, King TE, Lasky JA, Martinez FJ. 2012. Prednisone, azathioprine, and N-acetylcysteine for pulmonary fibrosis. *N Engl J Med* **366**:1968–77. doi:10.1056/NEJMoa1113354

Ishida Y, Kondo T, Takayasu T, Iwakura Y, Mukaida N. 2004. The essential involvement of cross-talk between IFN-gamma and TGF-beta in the skin wound-healing process. *J Immunol* **172**:1848–55. doi:10.4049/jimmunol.172.3.1848

Iwai Y, Hemmi H, Mizenina O, Kuroda S, Suda K, Steinman RM. 2008. An IFN-gamma-IL-

18 signaling loop accelerates memory CD8+ T cell proliferation. *PLoS One* **3**:e2404. doi:10.1371/journal.pone.0002404

Iwamoto I, Nakajima H, Endo H, Yoshida S. 1993. Interferon gamma regulates antigen-induced eosinophil recruitment into the mouse airways by inhibiting the infiltration of CD4+ T cells. *J Exp Med* **177**:573–6. doi:10.1084/jem.177.2.573

Janho Dit Hreich S, Hofman P, Vouret-Craviari V. 2023. The Role of IL-18 in P2RX7-Mediated Antitumor Immunity. *Int J Mol Sci* **24**. doi:10.3390/ijms24119235

Jenkins RG, Moore BB, Chambers RC, Eickelberg O, Königshoff M, Kolb M, Laurent GJ, Nanthakumar CB, Olman MA, Pardo A, Selman M, Sheppard D, Sime PJ, Tager AM, Tatler AL, Thannickal VJ, White ES. 2017. An Official American Thoracic Society Workshop Report: Use of Animal Models for the Preclinical Assessment of Potential Therapies for Pulmonary Fibrosis. *Am J Respir Cell Mol Biol* **56**:667–679. doi:10.1165/rcmb.2017-0096ST

Karasawa A, Kawate T. 2016. Structural basis for subtype-specific inhibition of the P2X7 receptor. *Elife* **5**. doi:10.7554/eLife.22153

Karasawa A, Michalski K, Mikhelzon P, Kawate T. 2017. The P2X7 receptor forms a dye-permeable pore independent of its intracellular domain but dependent on membrane lipid composition. *Elife* **6**. doi:10.7554/eLife.31186

Khalil N, O'Connor RN, Unruh HW, Warren PW, Flanders KC, Kemp A, Bereznay OH, Greenberg AH. 1991. Increased production and immunohistochemical localization of transforming growth factor-beta in idiopathic pulmonary fibrosis. *Am J Respir Cell Mol Biol* **5**:155–62. doi:10.1165/ajrcmb/5.2.155

King TE, Albera C, Bradford WZ, Costabel U, Hormel P, Lancaster L, Noble PW, Sahn SA, Szwarcberg J, Thomeer M, Valeyre D, du Bois RM, INSPIRE Study Group. 2009. Effect of interferon gamma-1b on survival in patients with idiopathic pulmonary fibrosis (INSPIRE): a multicentre, randomised, placebo-controlled trial. *Lancet (London, England)* **374**:222–8. doi:10.1016/S0140-6736(09)60551-1

Koutoulaki A, Langley M, Sloan AJ, Aeschlimann D, Wei X-Q. 2010. TNFalpha and TGF-beta1 influence IL-18-induced IFNgamma production through regulation of IL-18 receptor and T-bet expression. *Cytokine* **49**:177–84. doi:10.1016/j.cyto.2009.09.015

Kreuter M, Lee JS, Tzouvelekis A, Oldham JM, Molyneaux PL, Weycker D, Atwood M, Kirchgaessler K-U, Maher TM. 2021. Monocyte Count as a Prognostic Biomarker in Patients with Idiopathic Pulmonary Fibrosis. *Am J Respir Crit Care Med* **204**:74–81. doi:10.1164/rccm.202003-0669OC

Lasithiotaki I, Giannarakis I, Tsitoura E, Samara KD, Margaritopoulos GA, Choulaki C, Vasarmidi E, Tzanakis N, Voloudaki A, Sidiropoulos P, Siafakas NM, Antoniou KM. 2016. NLRP3 inflammasome expression in idiopathic pulmonary fibrosis and rheumatoid lung. *Eur Respir J* **47**:910–8. doi:10.1183/13993003.00564-2015

Lasithiotaki I, Tsitoura E, Samara KD, Trachalaki A, Charalambous I, Tzanakis N, Antoniou KM. 2018. NLRP3/Caspase-1 inflammasome activation is decreased in alveolar macrophages in patients with lung cancer. *PLoS One* **13**:e0205242. doi:10.1371/journal.pone.0205242

Laurence A, Tato CM, Davidson TS, Kanno Y, Chen Z, Yao Z, Blank RB, Meylan F, Siegel R, Hennighausen L, Shevach EM, O'shea JJ. 2007. Interleukin-2 signaling via STAT5 constrains T helper 17 cell generation. *Immunity* **26**:371–81. doi:10.1016/j.immuni.2007.02.009

Liu Y-Z, Saito S, Morris GF, Miller CA, Li J, Lefante JJ. 2019. Proportions of resting memory T cells and monocytes in blood have prognostic significance in idiopathic pulmonary fibrosis. *Genomics* **111**:1343–1350. doi:10.1016/j.ygeno.2018.09.006

Luzina IG, Todd NW, Iacono AT, Atamas SP. 2008. Roles of T lymphocytes in pulmonary

fibrosis. *J Leukoc Biol* **83**:237–44. doi:10.1189/jlb.0707504
Mavrogiannis E, Hagdorn QAJ, Bazioti V, Douwes JM, Van Der Feen DE, Oberdorf-Maass SU, Westerterp M, Berger RMF. 2022. Pirfenidone ameliorates pulmonary arterial pressure and neointimal remodeling in experimental pulmonary arterial hypertension by suppressing NLRP3 inflammasome activation. *Pulm Circ* **12**:e12101. doi:10.1002/pul2.12101
McCubbrey AL, Barthel L, Mohning MP, Redente EF, Mould KJ, Thomas SM, Leach SM, Danhorn T, Gibbings SL, Jakubzick C V, Henson PM, Janssen WJ. 2018. Deletion of c-FLIP from CD11bhi Macrophages Prevents Development of Bleomycin-induced Lung Fibrosis. *Am J Respir Cell Mol Biol* **58**:66–78. doi:10.1165/rcmb.2017-0154OC
Misharin A V, Morales-Nebreda L, Reyfman PA, Cuda CM, Walter JM, McQuattie-Pimentel AC, Chen C-I, Anekalla KR, Joshi N, Williams KJN, Abdala-Valencia H, Yacoub TJ, Chi M, Chiu S, Gonzalez-Gonzalez FJ, Gates K, Lam AP, Nicholson TT, Homan PJ, Soberanes S, Dominguez S, Morgan VK, Saber R, Shaffer A, Hinchcliff M, Marshall SA, Bharat A, Berdnikovs S, Bhorade SM, Bartom ET, Morimoto RI, Balch WE, Sznajder JI, Chandel NS, Mutlu GM, Jain M, Gottardi CJ, Singer BD, Ridge KM, Bagheri N, Shilatifard A, Budinger GRS, Perlman H. 2017. Monocyte-derived alveolar macrophages drive lung fibrosis and persist in the lung over the life span. *J Exp Med* **214**:2387–2404. doi:10.1084/jem.20162152
Morimoto Y, Hirahara K, Kiuchi M, Wada T, Ichikawa T, Kanno T, Okano M, Kokubo K, Onodera A, Sakurai D, Okamoto Y, Nakayama T. 2018. Amphiregulin-Producing Pathogenic Memory T Helper 2 Cells Instruct Eosinophils to Secrete Osteopontin and Facilitate Airway Fibrosis. *Immunity* **49**:134-150.e6. doi:10.1016/j.immuni.2018.04.023
Muñoz-Planillo R, Kuffa P, Martínez-Colón G, Smith BL, Rajendiran TM, Núñez G. 2013. K^+ efflux is the common trigger of NLRP3 inflammasome activation by bacterial toxins and particulate matter. *Immunity* **38**:1142–53. doi:10.1016/j.immuni.2013.05.016
Naccache J-M, Jouneau S, Didier M, Borie R, Cachanado M, Bourdin A, Reynaud-Gaubert M, Bonniaud P, Israël-Biet D, Prévot G, Hirschi S, Lebargy F, Marchand-Adam S, Bautin N, Traclet J, Gomez E, Leroy S, Gagnadoux F, Rivière F, Bergot E, Gondouin A, Blanchard E, Parrot A, Blanc F-X, Chabrol A, Dominique S, Gibelin A, Tazi A, Berard L, Brillet PY, Debray M-P, Rousseau A, Kerjouan M, Freynet O, Dombret M-C, Gamez A-S, Nieves A, Beltramo G, Pastré J, Le Borgne-Krams A, Dégot T, Launois C, Plantier L, Wémeau-Stervinou L, Cadranel J, Chenivesse C, Valeyre D, Crestani B, Cottin V, Simon T, Nunes H, EXAFIP investigators and the OrphaLung network. 2022. Cyclophosphamide added to glucocorticoids in acute exacerbation of idiopathic pulmonary fibrosis (EXAFIP): a randomised, double-blind, placebo-controlled, phase 3 trial. *Lancet Respir Med* **10**:26–34. doi:10.1016/S2213-2600(21)00354-4
Nakanishi Y, Horimasu Y, Yamaguchi K, Sakamoto S, Masuda T, Nakashima T, Miyamoto S, Iwamoto H, Ohshimo S, Fujitaka K, Hamada H, Hattori N. 2021. IL-18 binding protein can be a prognostic biomarker for idiopathic pulmonary fibrosis. *PLoS One* **16**:e0252594. doi:10.1371/journal.pone.0252594
Nakatani-Okuda A, Ueda H, Kashiwamura S-I, Sekiyama A, Kubota A, Fujita Y, Adachi S, Tsuji Y, Tanizawa T, Okamura H. 2005. Protection against bleomycin-induced lung injury by IL-18 in mice. *Am J Physiol Lung Cell Mol Physiol* **289**:L280-7. doi:10.1152/ajplung.00380.2004
Nörenberg W, Hempel C, Urban N, Sobottka H, Illes P, Schaefer M. 2011. Clemastine potentiates the human P2X7 receptor by sensitizing it to lower ATP concentrations. *J Biol Chem* **286**:11067–81. doi:10.1074/jbc.M110.198879
Okamura H, Tsutsi H, Komatsu T, Yutsudo M, Hakura A, Tanimoto T, Torigoe K, Okura T, Nukada Y, Hattori K. 1995. Cloning of a new cytokine that induces IFN-gamma production by T cells. *Nature* **378**:88–91. doi:10.1038/378088a0
Oku H, Shimizu T, Kawabata T, Nagira M, Hikita I, Ueyama A, Matsushima S, Torii M,

Arimura A. 2008. Antifibrotic action of pirfenidone and prednisolone: different effects on pulmonary cytokines and growth factors in bleomycin-induced murine pulmonary fibrosis. *Eur J Pharmacol* **590**:400–8. doi:10.1016/j.ejphar.2008.06.046

Park I-K, Letterio JJ, Gorham JD. 2007. TGF-beta 1 inhibition of IFN-gamma-induced signaling and Th1 gene expression in CD4+ T cells is Smad3 independent but MAP kinase dependent. *Mol Immunol* **44**:3283–90. doi:10.1016/j.molimm.2007.02.024

Patel AS, Lin L, Geyer A, Haspel JA, An CH, Cao J, Rosas IO, Morse D. 2012. Autophagy in idiopathic pulmonary fibrosis. *PLoS One* **7**:e41394. doi:10.1371/journal.pone.0041394

Peng R, Sridhar S, Tyagi G, Phillips JE, Garrido R, Harris P, Burns L, Renteria L, Woods J, Chen L, Allard J, Ravindran P, Bitter H, Liang Z, Hogaboam CM, Kitson C, Budd DC, Fine JS, Bauer CMT, Stevenson CS. 2013. Bleomycin induces molecular changes directly relevant to idiopathic pulmonary fibrosis: a model for “active” disease. *PLoS One* **8**:e59348. doi:10.1371/journal.pone.0059348

Penton-Rol G, Polentarutti N, Luini W, Borsatti A, Mancinelli R, Sica A, Sozzani S, Mantovani A. 1998. Selective inhibition of expression of the chemokine receptor CCR2 in human monocytes by IFN-gamma. *J Immunol* **160**:3869–73.

Perregaux DG, McNiff P, Laliberte R, Conklyn M, Gabel CA. 2000. ATP acts as an agonist to promote stimulus-induced secretion of IL-1 beta and IL-18 in human blood. *J Immunol* **165**:4615–23. doi:10.4049/jimmunol.165.8.4615

Pinar AA, Yuferov A, Gaspari TA, Samuel CS. 2020. Relaxin Can Mediate Its Anti-Fibrotic Effects by Targeting the Myofibroblast NLRP3 Inflammasome at the Level of Caspase-1. *Front Pharmacol* **11**:1201. doi:10.3389/fphar.2020.01201

Pippel A, Stolz M, Woltersdorf R, Kless A, Schmalzing G, Markwardt F. 2017. Localization of the gate and selectivity filter of the full-length P2X7 receptor. *Proc Natl Acad Sci U S A* **114**:E2156–E2165. doi:10.1073/pnas.1610414114

Prior C, Haslam PL. 1992. In vivo levels and in vitro production of interferon-gamma in fibrosing interstitial lung diseases. *Clin Exp Immunol* **88**:280–7. doi:10.1111/j.1365-2249.1992.tb03074.x

Puren AJ, Fantuzzi G, Dinarello CA. 1999. Gene expression, synthesis, and secretion of interleukin 18 and interleukin 1beta are differentially regulated in human blood mononuclear cells and mouse spleen cells. *Proc Natl Acad Sci U S A* **96**:2256–61. doi:10.1073/pnas.96.5.2256

Raghu G, Rochwerg B, Zhang Y, Garcia CAC, Azuma A, Behr J, Brozek JL, Collard HR, Cunningham W, Homma S, Johkoh T, Martinez FJ, Myers J, Protzko SL, Richeldi L, Rind D, Selman M, Theodore A, Wells AU, Hoogsteden H, Schünemann HJ, American Thoracic Society, European Respiratory society, Japanese Respiratory Society, Latin American Thoracic Association. 2015. An Official ATS/ERS/JRS/ALAT Clinical Practice Guideline: Treatment of Idiopathic Pulmonary Fibrosis. An Update of the 2011 Clinical Practice Guideline. *Am J Respir Crit Care Med* **192**:e3-19. doi:10.1164/rccm.201506-1063ST

Riteau N, Gasse P, Fauconnier L, Gombault A, Couegnat M, Fick L, Kanellopoulos J, Quesniaux VFJ, Marchand-Adam S, Crestani B, Ryffel B, Couillin I. 2010. Extracellular ATP Is a Danger Signal Activating P2X 7 Receptor in Lung Inflammation and Fibrosis. *Am J Respir Crit Care Med* **182**:774–783. doi:10.1164/rccm.201003-0359OC

Sáez PJ, Vargas P, Shoji KF, Harcha PA, Lennon-Duménil A-M, Sáez JC. 2017. ATP promotes the fast migration of dendritic cells through the activity of pannexin 1 channels and P2X7 receptors. *Sci Signal* **10**. doi:10.1126/scisignal.aah7107

Scott MKD, Quinn K, Li Q, Carroll R, Warsinske H, Vallania F, Chen S, Carns MA, Aren K, Sun J, Koloms K, Lee J, Baral J, Kropski J, Zhao H, Herzog E, Martinez FJ, Moore BB, Hinchcliff M, Denny J, Kaminski N, Herazo-Maya JD, Shah NH, Khatri P. 2019. Increased monocyte count as a cellular biomarker for poor outcomes in fibrotic diseases: a

retrospective, multicentre cohort study. *Lancet Respir Med* **7**:497–508. doi:10.1016/S2213-2600(18)30508-3

Sharawy MH, Serrya MS. 2020. Pirfenidone attenuates gentamicin-induced acute kidney injury by inhibiting inflammasome-dependent NLRP3 pathway in rats. *Life Sci* **260**:118454. doi:10.1016/j.lfs.2020.118454

Shenderov K, Collins SL, Powell JD, Horton MR. 2021. Immune dysregulation as a driver of idiopathic pulmonary fibrosis. *J Clin Invest* **131**. doi:10.1172/JCI143226

Skaria SD, Yang J, Condos R, Smaldone GC. 2015. Inhaled Interferon and Diffusion Capacity in Idiopathic Pulmonary Fibrosis (IPF). *Sarcoidosis, Vasc Diffus lung Dis Off J WASOG* **32**:37–42.

Smaldone GC. 2018. Repurposing of gamma interferon via inhalation delivery. *Adv Drug Deliv Rev* **133**:87–92. doi:10.1016/j.addr.2018.06.004

Sobecki M, Chen J, Krzywinska E, Nagarajan S, Fan Z, Nelius E, Monné Rodriguez JM, Seehusen F, Hussein A, Moschini G, Hajam EY, Kiran R, Gotthardt D, Debbache J, Badoual C, Sato T, Isagawa T, Takeda N, Tanchot C, Tartour E, Weber A, Werner S, Loffing J, Sommer L, Sexl V, Münz C, Feghali-Bostwick C, Pachera E, Distler O, Snedeker J, Jamora C, Stockmann C. 2022. Vaccination-based immunotherapy to target profibrotic cells in liver and lung. *Cell Stem Cell* **29**:1459-1474.e9. doi:10.1016/j.stem.2022.08.012

Spagnolo P, Kropski JA, Jones MG, Lee JS, Rossi G, Karampitsakos T, Maher TM, Tzouvelekis A, Ryerson CJ. 2021. Idiopathic pulmonary fibrosis: Disease mechanisms and drug development. *Pharmacol Ther* **222**:107798. doi:10.1016/j.pharmthera.2020.107798

Stokes L, Bidula S, Bibič L, Allum E. 2020. To Inhibit or Enhance? Is There a Benefit to Positive Allosteric Modulation of P2X Receptors? *Front Pharmacol* **11**:627. doi:10.3389/fphar.2020.00627

Su W-J, Zhang T, Jiang C-L, Wang W. 2018. Clemastine Alleviates Depressive-Like Behavior Through Reversing the Imbalance of Microglia-Related Pro-inflammatory State in Mouse Hippocampus. *Front Cell Neurosci* **12**. doi:10.3389/fncel.2018.00412

Surprenant A, Rassendren F, Kawashima E, North RA, Buell G. 1996. The cytolytic P2Z receptor for extracellular ATP identified as a P2X receptor (P2X7). *Science (80-)* **272**:735–738. doi:10.1126/science.272.5262.735

Sutton CE, Lalor SJ, Sweeney CM, Brereton CF, Lavelle EC, Mills KHG. 2009. Interleukin-1 and IL-23 induce innate IL-17 production from gammadelta T cells, amplifying Th17 responses and autoimmunity. *Immunity* **31**:331–41. doi:10.1016/j.immuni.2009.08.001

Ulloa L, Doody J, Massagué J. 1999. Inhibition of transforming growth factor-beta/SMAD signalling by the interferon-gamma/STAT pathway. *Nature* **397**:710–3. doi:10.1038/17826

Varga J, Olsen A, Herhal J, Constantine G, Rosenbloom J, Jimenez SA. 1990. Interferon-gamma reverses the stimulation of collagen but not fibronectin gene expression by transforming growth factor-beta in normal human fibroblasts. *Eur J Clin Invest* **20**:487–93. doi:10.1111/j.1365-2362.1990.tb01890.x

Watanabe A, Sohail MA, Gomes DA, Hashmi A, Nagata J, Sutterwala FS, Mahmood S, Jhandier MN, Shi Y, Flavell RA, Mehal WZ. 2009. Inflammasome-mediated regulation of hepatic stellate cells. *Am J Physiol Gastrointest Liver Physiol* **296**:G1248-57. doi:10.1152/ajpgi.90223.2008

Wei Y, Zhao L. 2014. Passive lung-targeted drug delivery systems via intravenous administration. *Pharm Dev Technol* **19**:129–36. doi:10.3109/10837450.2012.757782

Wilson MS, Madala SK, Ramalingam TR, Gochuico BR, Rosas IO, Cheever AW, Wynn TA. 2010. Bleomycin and IL-1beta-mediated pulmonary fibrosis is IL-17A dependent. *J Exp Med* **207**:535–52. doi:10.1084/jem.20092121

Xu J, Mora AL, LaVoy J, Brigham KL, Rojas M. 2006. Increased bleomycin-induced lung injury in mice deficient in the transcription factor T-bet. *Am J Physiol Lung Cell Mol Physiol*

291:L658-67. doi:10.1152/ajplung.00006.2006

Yuan W, Yufit T, Li L, Mori Y, Chen SJ, Varga J. 1999. Negative modulation of alpha1(I) procollagen gene expression in human skin fibroblasts: transcriptional inhibition by interferon-gamma. *J Cell Physiol* **179**:97–108. doi:10.1002/(SICI)1097-4652(199904)179:1<97::AID-JCP12>3.0.CO;2-E

Zhang L-M, Zhang Y, Fei C, Zhang J, Wang L, Yi Z-W, Gao G. 2019. Neutralization of IL-18 by IL-18 binding protein ameliorates bleomycin-induced pulmonary fibrosis via inhibition of epithelial-mesenchymal transition. *Biochem Biophys Res Commun* **508**:660–666. doi:10.1016/j.bbrc.2018.11.129

Table1. Antibodies used in this study

Antibody	Dilution	Fluorochrome	Clone	Reference	Supplier
CD16/CD32	1/100		2.4G2	553142	BD Biosciences
CD3ε	1/100	PerCP-Cy5.5	145-2611	551163	
NK1.1	1/100	PE-CF594	PK136	562864	
CD11c	1/100	PE-Cy7	HL3	558079	
Ly6G	1/100	AF700	1A8	561236	
Ly6C	1/100	V450	AL-21	560594	
SiglecF	1/50	BV605	E50-2440	740388	
CD4	1/100	BV711	RM4-5	563726	
CD8α	1/100	BV650	53-6.7	100741	
CD45.2	1/100	BV786	104	563686	
CD45	1/100	BUV395	30-F11	564279	
γδ TCR	1/100	PE	GL3	553178	
IFNγ	1/100	APC	XMG1.2	554413	
IL-17A	1/100	AF700	TC11-18H10	561718	
I-A/I-E	1/100	APCfire750	M5/114.15.2	107651	Biolegend
CD64	1/20	PE	X54-5/7.1	139303	
P2RX7	1/8	PE	1F11	148706	
CD140a	1/100	PE	APA5	135905	
CD11b	1/400	APC	M1/70	17-0112-82	eBiosciences
Foxp3	1/100	PE	FJK16S	12-5773-82	
NLRP3	1/1000		Cryo-2	AG-20B-0014	Adipogen
ACTIN BETA	1/60000		monoclonal	VMA00048	Biorad
IL-18	1/250		polyclonal	5180R-100	Biovision

Figure legends

Figure 1. The P2RX7/IL-18/IFN-γ pathway is downregulated in IPF

(A) Heatmap of mRNA expression of P2RX7 in control and IPF patients with a cluster of fibrosis-associated genes. Raw p-values are shown (Limma). P-values were determined by Spearman test. **(B)** mRNA expression of *P2RX7, IL18, IL18R1, IL18RAP* and *IFNG* between control and IPF patients from 213 individuals, corresponding to 91 controls and 122 IPF patients. P-values were determined by Two-tailed unpaired t-test or Mann-Whitney t-test. ***$p < 0.001$, ****$p < 0.0001$. **(C)** Gene set enrichment analysis (GSEA) plot associating P2RX7 mRNA levels from IPF patients with three immunological signatures. The green line represents the enrichment score and the black lines the specific signature-associated genes. NES: Normalized enrichment score, p-values (bilateral Kolmogorov–Smirnov), and false discovery rate (FDR) are shown.

Figure 2. HEI3090 inhibits lung fibrosis progression

(A) Experimental design. WT mice were given 2.5 U/kg of bleomycin by i.n. route. At the end of the inflammatory phase (d7), 1.5 mg/kg of HEI3090 or vehicle were given daily until day 21. **(B)** Representative images of lung sections at day 21 after treatment stained with H&E and Sirius Red, Scale bar= 100 µm. **(C)** Fibrosis score assessed by the Ashcroft method. P-values were determined by Two-tailed unpaired t-test. **(D)** Quantification of fibroblasts/myofibroblasts in non-immune cell subset. P-values were determined by Two-tailed Mann-Whitney test. **(E)** Representative images of lung sections at day 21 after treatment stained with Sirius Red, Scale bar= 100 µm. **(F)** Collagen levels in whole lung of mice assessed on Sirius Red-polarized images. P-values were determined by Two-tailed unpaired t-test. **(G)** Experimental design. WT mice were given 2.5 U/kg of bleomycin by i.n. route. 1.5 mg/kg of HEI3090 or vehicle were given daily until day 14. **(H)** Representative images of lung sections at day 14 after treatment

stained with H&E, Scale bar= 100 µm. **(I)** Fibrosis score assessed by the Ashcroft method. P-values were determined by Two-tailed unpaired t-test. **(J)** Quantification of fibroblasts/myofibroblasts in non-immune cell subset. P-values were determined by Two-tailed Mann-Whitney test. **(K)** Representative images of lung sections at day 14 after treatment stained with Sirius Red, Scale bar= 100 µm. **(L)** Collagen levels in whole lung of mice assessed on Sirius Red-polarized images. P-values were determined by Two-tailed Mann-Whitney test. (M) *P2rx7* KO mice were given 2.5 U/kg of bleomycin by i.n. route. 1.5 mg/kg of HEI3090 or vehicle were given daily until day 14. Fibrosis score assessed by the Ashcroft method is showed. P-values were determined by Two-tailed Mann-Whitney test. For all analyses, the violin plot illustrates the distribution of Ashcroft scores across indicated groups. The width of the violin at each point represents the density of data, and the central line indicates the median expression level. Each point represents one biological replicate. *$p < 0.05$, **$p < 0.01$. WT: Wildtype, BLM: bleomycin, i.p.: intraperitoneal, i.n.: intranasal, H&E: hematoxylin & eosin, AU: arbitrary units.

Figure 3. HEI3090 favors an anti-fibrotic immune signature in the lungs

WT mice were given 2.5 U/kg of bleomycin by i.n. route and treated daily i.p. with 1.5 mg/kg of HEI3090 or Vehicle. Lungs were analyzed by flow cytometry at day 14. **(A)** Contour plot of IFN-γ and IL-17A producing T cells ($CD3^+NK1.1^-$) (left) and ratio of IFN-γ over IL-17A in T cells ($CD3^+NK1.1^-$) (right). P-values were determined by Two-tailed Mann-Whitney test. **(B)** Percentage of IFN-γ producing $CD4^+$ and $CD8^+$ T cells. P-values were determined by Two-tailed Mann-Whitney test. **(C)** Percentage and GMFI of IL-$17A^+$ cells of $CD4^+$ T cells ($CD3^+CD4^+NK1.1^-$). P-values were determined by Two-tailed Mann-Whitney test. **(D)** Percentage and GMFI of TGFβ in $CD45^+$ cells. P-values were determined by Two-tailed Mann-Whitney test. **(E)** Dotplot showing lung inflammatory monocytes, gated on $lineage^-CD11c^-$

CD11b^{+} cells (left) and percentage of lung inflammatory monocytes (Ly6C^{high}Ly6G^{-}) (right). P-values were determined by Two-tailed Mann-Whitney test. **(F)** Percentage of alveolar macrophages (CD11c^{+}SiglecF^{+}), p-values were determined by Two-tailed unpaired t-test and **(G)** lung eosinophils (CD11b^{+}SiglecF^{+}CD11c^{-}), p-values were determined by Two-tailed Mann-Whitney test. **(A-G),** The violin plot illustrates the distribution of Ashcroft scores across indicated groups. The width of the violin at each point represents the density of data, and the central line indicates the median expression level. Each point represents one biological replicate. *$p < 0.05$, **$p < 0.01$. GMFI: geometric mean fluorescence intensity. i.n.: intranasal, i.p.: intraperitoneal.

Figure 4. The P2RX7/NLRP3/IL-18 pathway in immune cells is required for HEI3090's antifibrotic effect

(A) Experimental design. *p2rx7*$^{-/-}$ mice were given 3.106 WT, nlrp3-/- or il18-/- splenocytes i.v. one day prior to BLM delivery (i.n. 2.5 U/kg). Mice were treated daily i.p. with 1.5 mg/kg HEI3090 or vehicle for 14 days**. (B,E,H)** Representative images of lung sections at day 14 after treatment stained with H&E and Sirius Red, scale bar= 100 µm. **(C, F, I),** Fibrosis score assessed by the Ashcroft method and **(D, G, J),** Collagen fiber intensity. **(C)** WT splenocytes, p-values were determined by Two-tailed Mann-Whitney test. **(D)** WT splenocytes, p-values were determined by Two-tailed unpaired t-test. **(F, G)** *nlrp3*$^{-/-}$ splenocytes, p-values were determined by Two-tailed Mann-Whitney test. **(I, J)** *il18*$^{-/-}$ splenocytes, p-values were determined by Two-tailed Mann-Whitney test. **(K)** IL-18 levels in sera of WT BLM-induced mice at day 14. P-values were determined by Two-tailed unpaired t-test. **(L)** Ratio of IFN-γ over IL-17A in lung T cells (CD3+NK1.1-) of WT mice neutralized for IL-18 or not (isotype control) every 3 days. P-values were determined by one-way ANOVA with tukey's multiple comparisons test. For all analyses, the violin plot illustrates the distribution of Ashcroft scores

across indicated groups. The width of the violin at each point represents the density of data, and the central line indicates the median expression level. Each point represents one biological replicate. *$p < 0.05$, **$p < 0.01$ WT: Wildtype, BLM: bleomycin, i.p.: intraperitoneal, i.n.: intranasal, i.v.: intravenous, H&E: hematoxylin & eosin.

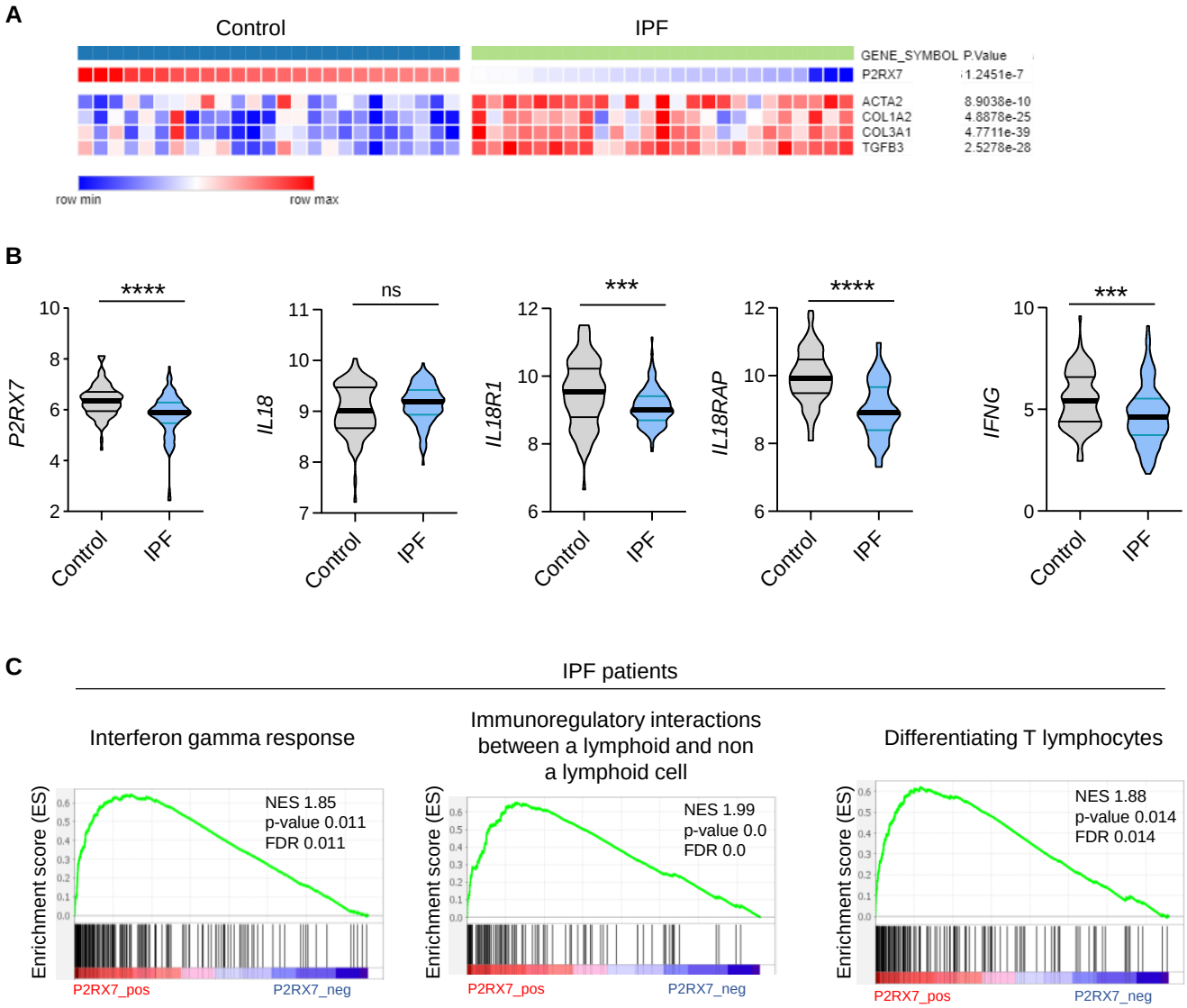

Figure 1 : The P2RX7/IL-18/IFN-γ pathway is downregulated in IPF

(A) Heatmap of mRNA expression of P2RX7 in control and IPF patients with a cluster of fibrosis-associated genes. Raw p-values are shown (Limma). P-values were determined by Spearman test. **(B)** mRNA expression of P2RX7, IL18, IL18R1, IL18RAP and IFNG between control and IPF patients from 213 individuals, corresponding to 91 controls and 122 IPF patients. P-values were determined by Two-tailed unpaired t-test or Mann-Whitney t-test. ***$p < 0.001$, ****$p < 0.0001$. **(C)** Gene set enrichment analysis (GSEA) plot associating P2RX7 mRNA levels from IPF patients with three immunological signatures. The green line represents the enrichment score and the black lines the specific signature-associated genes. NES: Normalized enrichment score, p-values (bilateral Kolmogorov–Smirnov), and false discovery rate (FDR) are shown.

Fig2

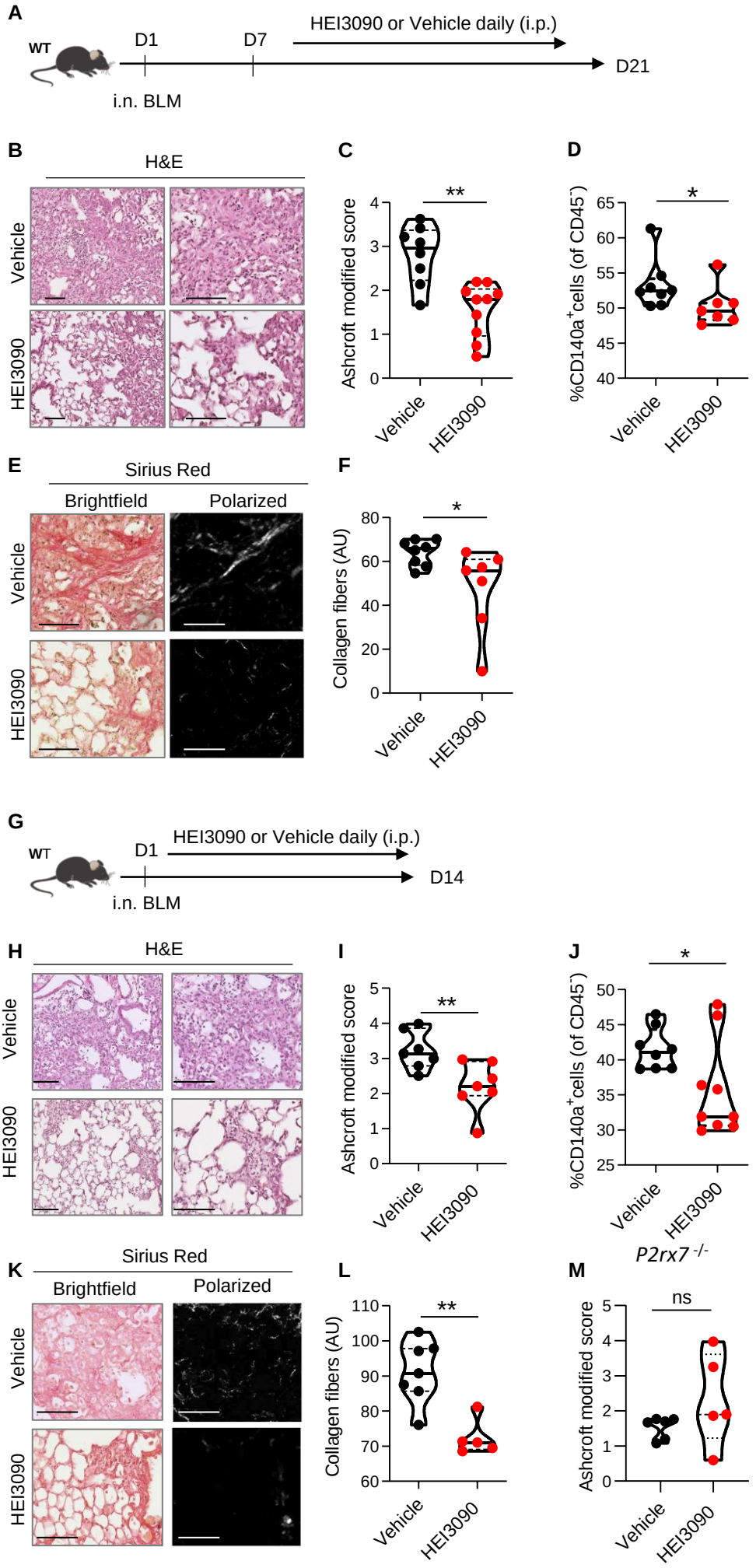
A
WT
D1
D7
HEI3090 or Vehicle daily (i.p.)
D21
i.n. BLM
B
H&E
Vehicle
HEI3090
C
Ashcroft modified score
**
Vehicle
HEI3090
D
%CD140a+cells (of CD45-)
*
Vehicle
HEI3090
E
Sirius Red
Brightfield
Polarized
Vehicle
HEI3090
F
Collagen fibers (AU)
*
Vehicle
HEI3090
G
WT
D1
HEI3090 or Vehicle daily (i.p.)
D14
i.n. BLM
H
H&E
Vehicle
HEI3090
I
Ashcroft modified score
**
Vehicle
HEI3090
J
%CD140a+cells (of CD45-)
*
Vehicle
HEI3090
P2rx7 -/-
K
Sirius Red
Brightfield
Polarized
Vehicle
HEI3090
L
Collagen fibers (AU)
**
Vehicle
HEI3090
M
Ashcroft modified score
ns
Vehicle
HEI3090

Figure 2 : HEI3090 attenuates lung fibrosis progression

(A) Experimental design. WT mice were given 2.5 U/kg of bleomycin by i.n. route. At the end of the inflammatory phase (d7), 1.5 mg/kg of HEI3090 or vehicle were given daily until day 21. (**B)** Representative images of lung sections at day 21 after treatment stained with H&E and Sirius Red, Scale bar= 100 µm. **(C)** Fibrosis score assessed by the Ashcroft method. P-values were determined by Two-tailed unpaired t-test. **(D)** Quantification of fibroblasts/myofibroblasts in non-immune cell subset. P-values were determined by Two-tailed Mann-Whitney test. **(E)** Representative images of lung sections at day 21 after treatment stained with Sirius Red, Scale bar= 100 µm. **(F)** Collagen levels in whole lung of mice assessed on Sirius Red-polarized images. P-values were determined by Two-tailed unpaired t-test. **(G)** Experimental design. WT mice were given 2.5 U/kg of bleomycin by i.n. route. 1.5 mg/kg of HEI3090 or vehicle were given daily until day 14. **(H)** Representative images of lung sections at day 14 after treatment stained with H&E, Scale bar= 100 µm. **(I)** Fibrosis score assessed by the Ashcroft method. P-values were determined by Two-tailed unpaired t-test. **(J)** Quantification of fibroblasts/myofibroblasts in non-immune cell subset. P-values were determined by Two-tailed Mann-Whitney test. **(K)** Representative images of lung sections at day 14 after treatment stained with Sirius Red, Scale bar= 100 µm. **(L)** Collagen levels in whole lung of mice assessed on Sirius Red-polarized images. P-values were determined by Two-tailed Mann-Whitney test. **(M)** P2rx7 KO mice were given 2.5 U/kg of bleomycin by i.n. route. 1.5 mg/kg of HEI3090 or vehicle were given daily until day 14. Fibrosis score assessed by the Ashcroft method is showed. P-values were determined by Two-tailed Mann-Whitney test. For all analyses, the violin plot illustrates the distribution of Ashcroft scores across indicated groups. The width of the violin at each point represents the density of data, and the central line indicates the median expression level. Each point represents one biological replicate. $*p < 0.05$, $**p < 0.01$. WT: Wildtype, BLM: bleomycin, i.p.: intraperitoneal, i.n.: intranasal, H&E: hematoxylin & eosin, AU: arbitrary units.

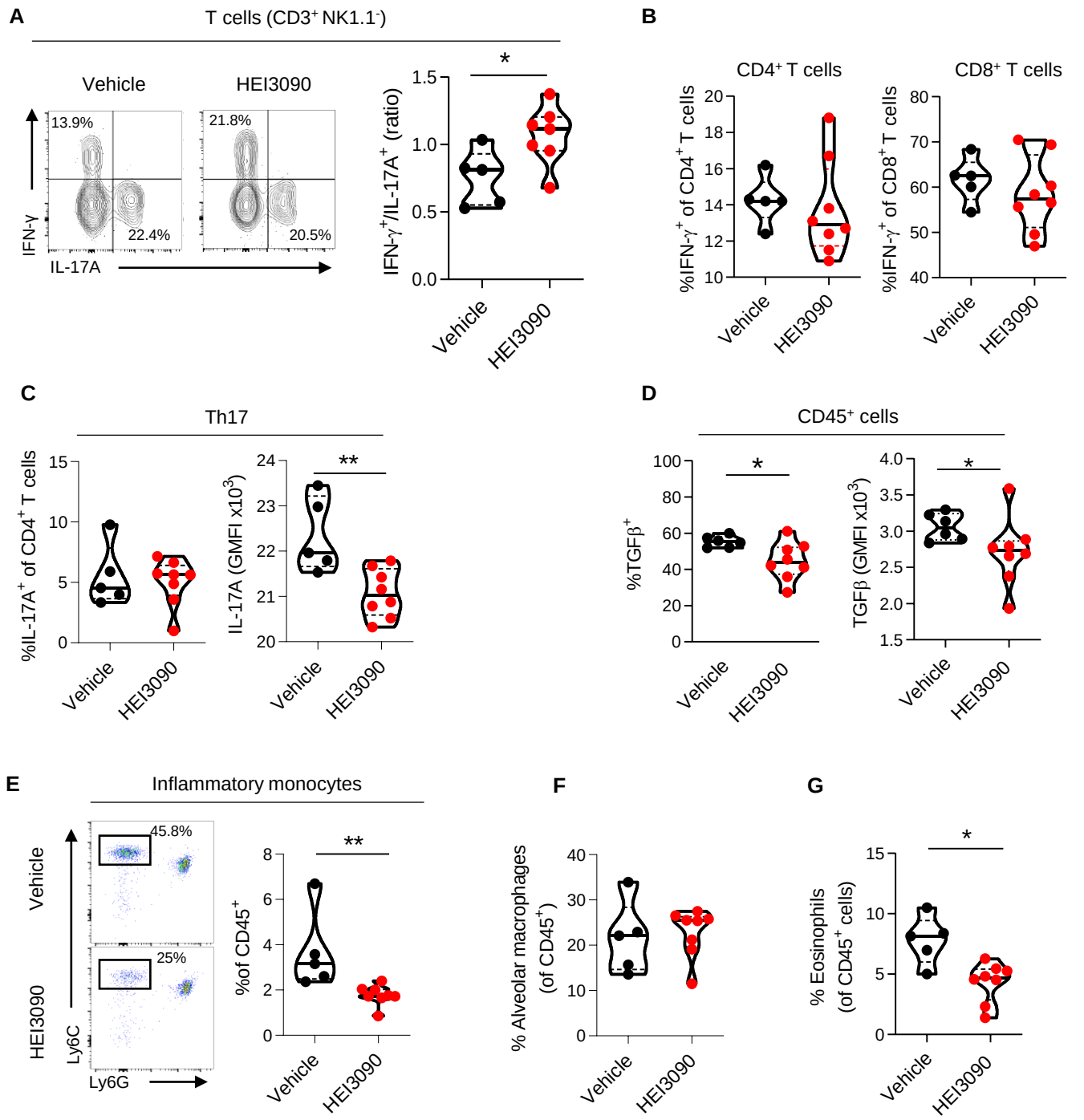

Figure 3 : HEI3090 favors an anti-fibrotic immune signature in the lungs

WT mice were given 2.5 U/kg of bleomycin by i.n. route and treated daily i.p. with 1.5 mg/kg of HEI3090 or Vehicle. Lungs were analyzed by flow cytometry at day 14. **(A)** Contour plot of IFN-γ and IL-17A producing T cells (CD3+NK1.1-) (left) and ratio of IFN-γ over IL-17A in T cells (CD3+NK1.1-) (right). P-values were determined by Two-tailed Mann-Whitney test. **(B)** Percentage of IFN-γ producing CD4+ and CD8+ T cells. P-values were determined by Two-tailed Mann-Whitney test. **(C)** Percentage and GMFI of IL-17A+ cells of CD4+ T cells (CD3+CD4+NK1.1-). P-values were determined by Two-tailed Mann-Whitney test. **(D)** Percentage and GMFI of TGFβ in CD45+ cells. P-values were determined by Two-tailed Mann-Whitney test. **(E)** Dotplot showing lung inflammatory monocytes, gated on lineage-CD11c-CD11b+ cells (left) and percentage of lung inflammatory monocytes (Ly6ChighLy6G-) (right). P-values were determined by Two-tailed Mann-Whitney test. **(F)** Percentage of alveolar macrophages (CD11c+SiglecF+), p-values were determined by Two-tailed unpaired t-test and **(G)** lung eosinophils (CD11b+SiglecF+CD11c-), p-values were determined by Two-tailed Mann-Whitney test. **(A-G),** The violin plot illustrates the distribution of Ashcroft scores across indicated groups. The width of the violin at each point represents the density of data, and the central line indicates the median expression level. Each point represents one biological replicate. *$p < 0.05$, **$p < 0.01$. GMFI: geometric mean fluorescence intensity. i.n.: intranasal, i.p.: intraperitoneal.

Fig4

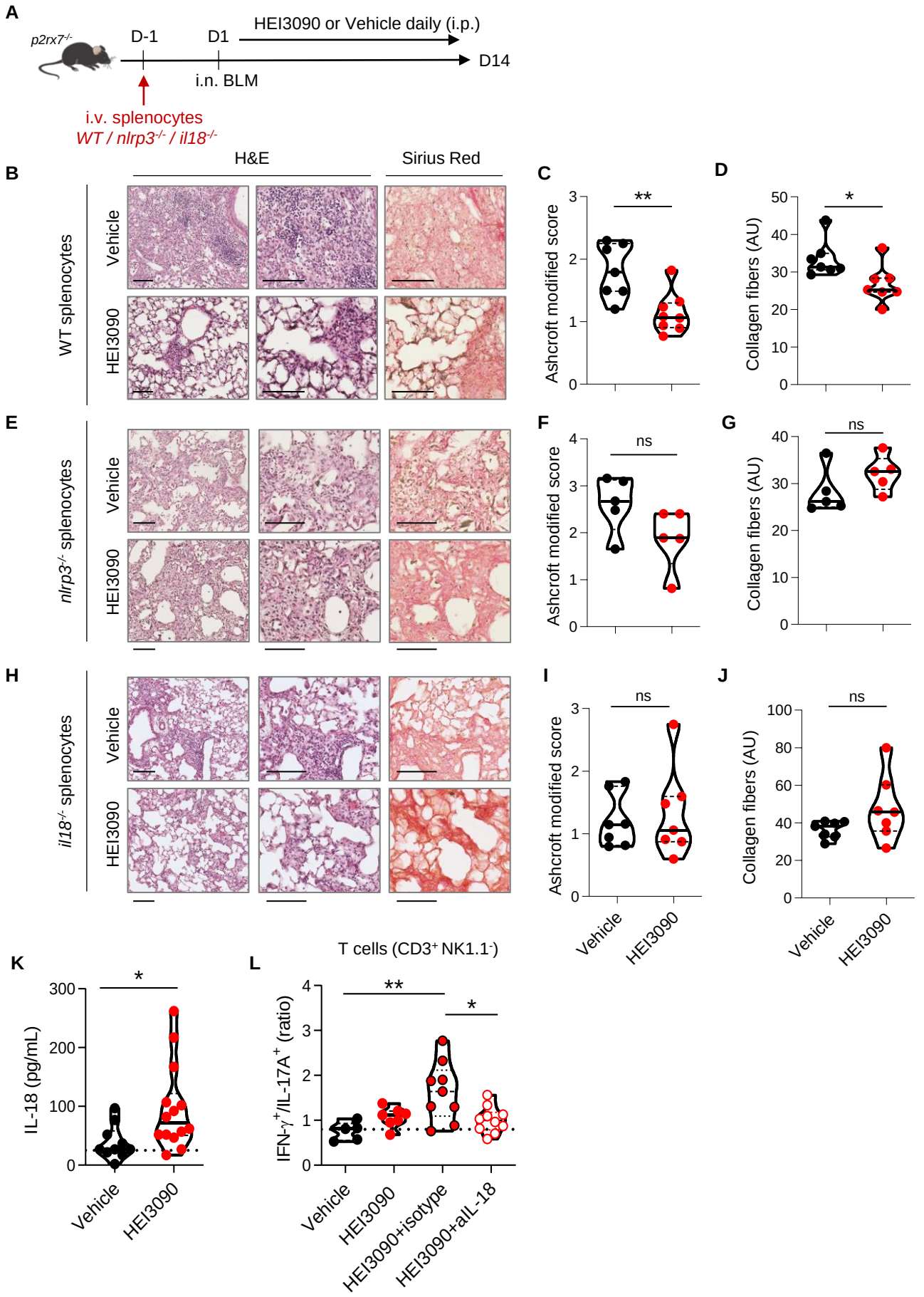
A
p2rx7-/-
D-1
D1
HEI3090 or Vehicle daily (i.p.)
D14
i.n. BLM
i.v. splenocytes
WT / nlrp3-/- / il18-/-
B
H&E
Sirius Red
WT splenocytes
Vehicle
HEI3090
C
Ashcroft modified score
**
D
Collagen fibers (AU)
*
E
nlrp3-/- splenocytes
F
ns
G
H
il18-/- splenocytes
I
J
Vehicle
HEI3090
K
IL-18 (pg/mL)
L
T cells (CD3+ NK1.1-)
IFN-γ+/IL-17A+ (ratio)
HEI3090+isotype
HEI3090+aIL-18

Figure 4: The P2RX7/NLRP3/IL-18 pathway in immune cells is required for HEI3090's antifibrotic effect

(A) Experimental design. p2rx7-/- mice were given 3.106 WT, nlrp3-/- or il18-/- splenocytes i.v. one day prior to BLM delivery (i.n. 2.5 U/kg). Mice were treated daily i.p. with 1.5 mg/kg HEI3090 or vehicle for 14 days. **(B,E,H)** Representative images of lung sections at day 14 after treatment stained with H&E and Sirius Red, scale bar= 100 µm. **(C, F, I)** Fibrosis score assessed by the Ashcroft method and **(D, G, J)** Collagen fiber intensity. **(C)** WT splenocytes, p-values were determined by Two-tailed Mann-Whitney test. **(D)** WT splenocytes, p-values were determined by Two-tailed unpaired t-test. **(F, G)** nlrp3-/- splenocytes, p-values were determined by Two-tailed Mann-Whitney test. **(I, J)** il18-/- splenocytes, p-values were determined by Two-tailed Mann-Whitney test. **(K)** IL-18 levels in sera of WT BLM-induced mice at day 14. P-values were determined by Two-tailed unpaired t-test. **(L)** Ratio of IFN-γ over IL-17A in lung T cells (CD3+NK1.1-) of WT mice neutralized for IL-18 or not (isotype control) every 3 days. P-values were determined by one-way ANOVA with Tukey's multiple comparisons test. For all analyses, the violin plot illustrates the distribution of Ashcroft scores across indicated groups. The width of the violin at each point represents the density of data, and the central line indicates the median expression level. Each point represents one biological replicate. *$p < 0.05$, **$p < 0.01$ WT: Wildtype, BLM: bleomycin, i.p.: intraperitoneal, i.n.: intranasal, i.v.: intravenous, H&E: hematoxylin & eosin.

Supp Fig1

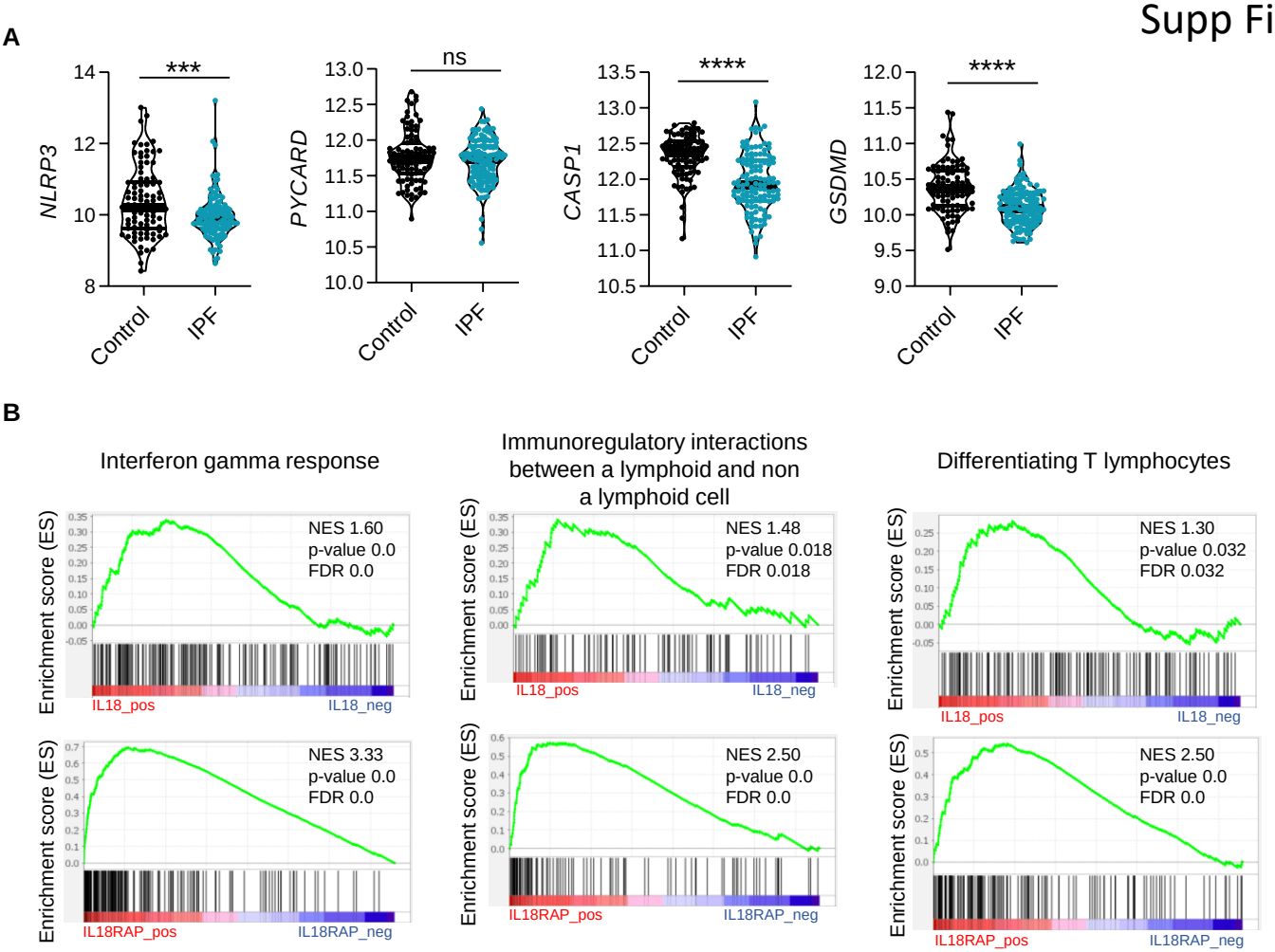

Supplemental Figure 1 : The components of the NLRP3 inflammasome are downregulated in IPF

(A) mRNA expression of *NLRP3, PYCARD, CASP1* and *GSDMD* between control and IPF patients from 213 individuals, corresponding to 91 controls and 122 IPF patients. P-values were determined by Two-tailed unpaired t-test or Mann-Whitney t-test. ***$p < 0.001$, ****$p < 0.0001$. **(B)** Gene set enrichment analysis (GSEA) plot associating P2RX7 mRNA levels from IPF patients with three immunological signatures. The green line represents the enrichment score and the black lines the specific signature-associated genes. NES: Normalized enrichment score. P-values (bilateral Kolmogorov–Smirnov), and false discovery rate (FDR) are shown.

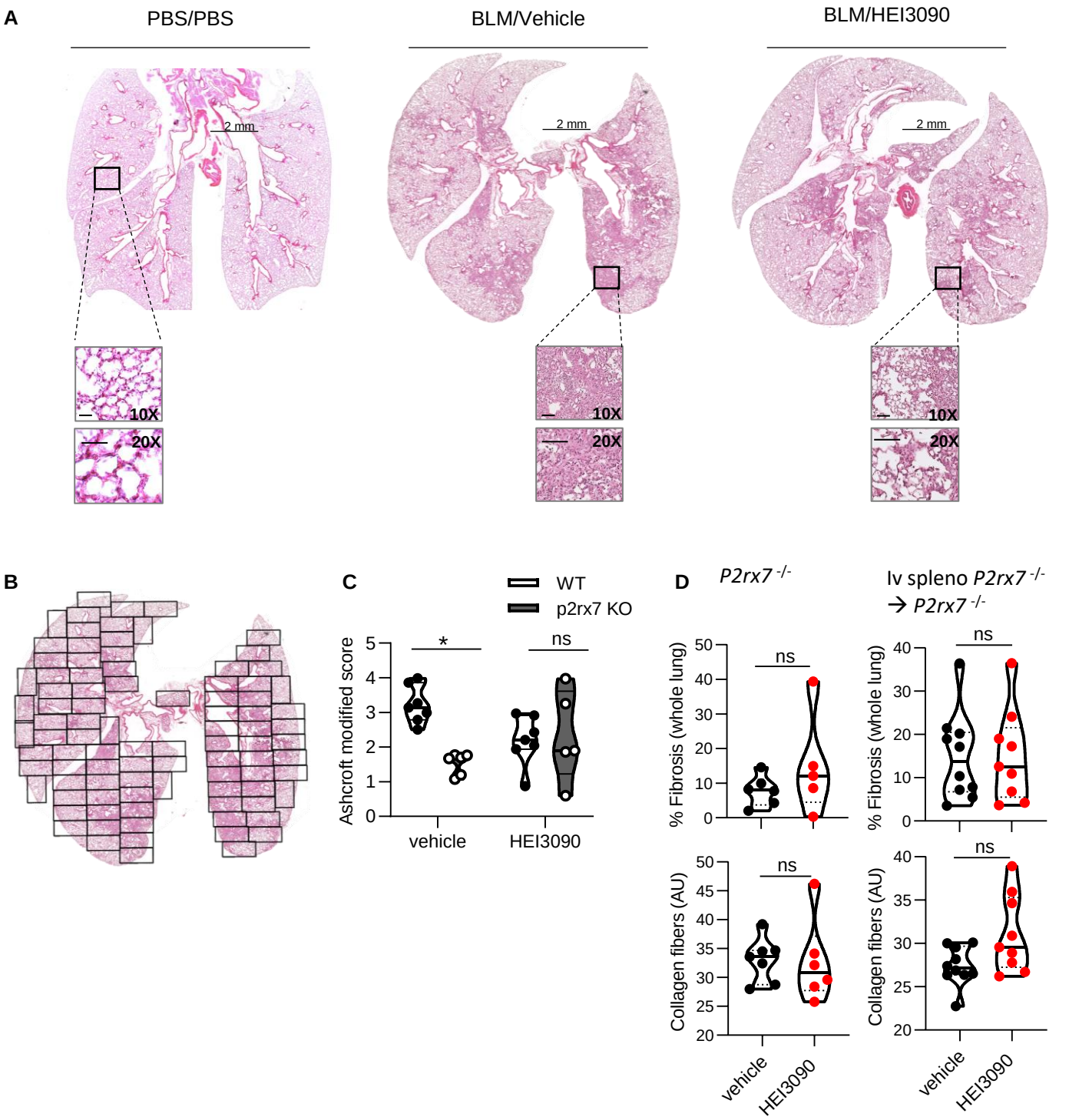

Supplemental Figure 2: HEI3090 treatment limits lung fibrosis progression

WT mice were given PBS or 2.5 U/kg of bleomycin by i.n. route. At the end of the inflammatory phase, 1.5 mg/kg of HEI3090 or vehicle were given daily until day 21. **(A)** Whole lung images at day 21 after treatment stained with H&E, Scale bar at 10X and 20X= 100 µm. **(B)** Whole lungs were divided in their entirety in several fields as shown to evaluate fibrosis severity using the Ashcroft method. The fibrosis score is the mean of all fields. **(C)** BLM-inhaled WT and P2rx7 KO mice were treated or not with HEI3090. At D14, whole lungs were removed, fixed in formol, and stained with H&E and lung fibrosis was scored. P-values were determined by two-way ANOVA with Bonferroni's multiple comparisons. **(D)** BLM-treated *p2rx7*$^{-/-}$ or *p2rx7*$^{-/-}$ adoptively transferred with *p2rx7*$^{-/-}$ splenocytes mice received HEI3090 for 14 days started at day 1. Whole lungs were removed, fixed and stained with Sirius red. The percentage of fibrosis in whole lung (up panel) was quantified concomitantly with the collagen quantification (lower panel) as described in the Material and Method section. P-values were determined by Two-tailed unpaired t-test. For all figures, the violin plot illustrates the distribution of Ashcroft scores across or collagen fibers intensity of indicated groups. The width of the violin at each point represents the density of data, and the central line indicates the median expression level. Each point represents one biological replicate. *$p < 0.05$, **$p < 0.01$, ns not significant.

Supp Fig3

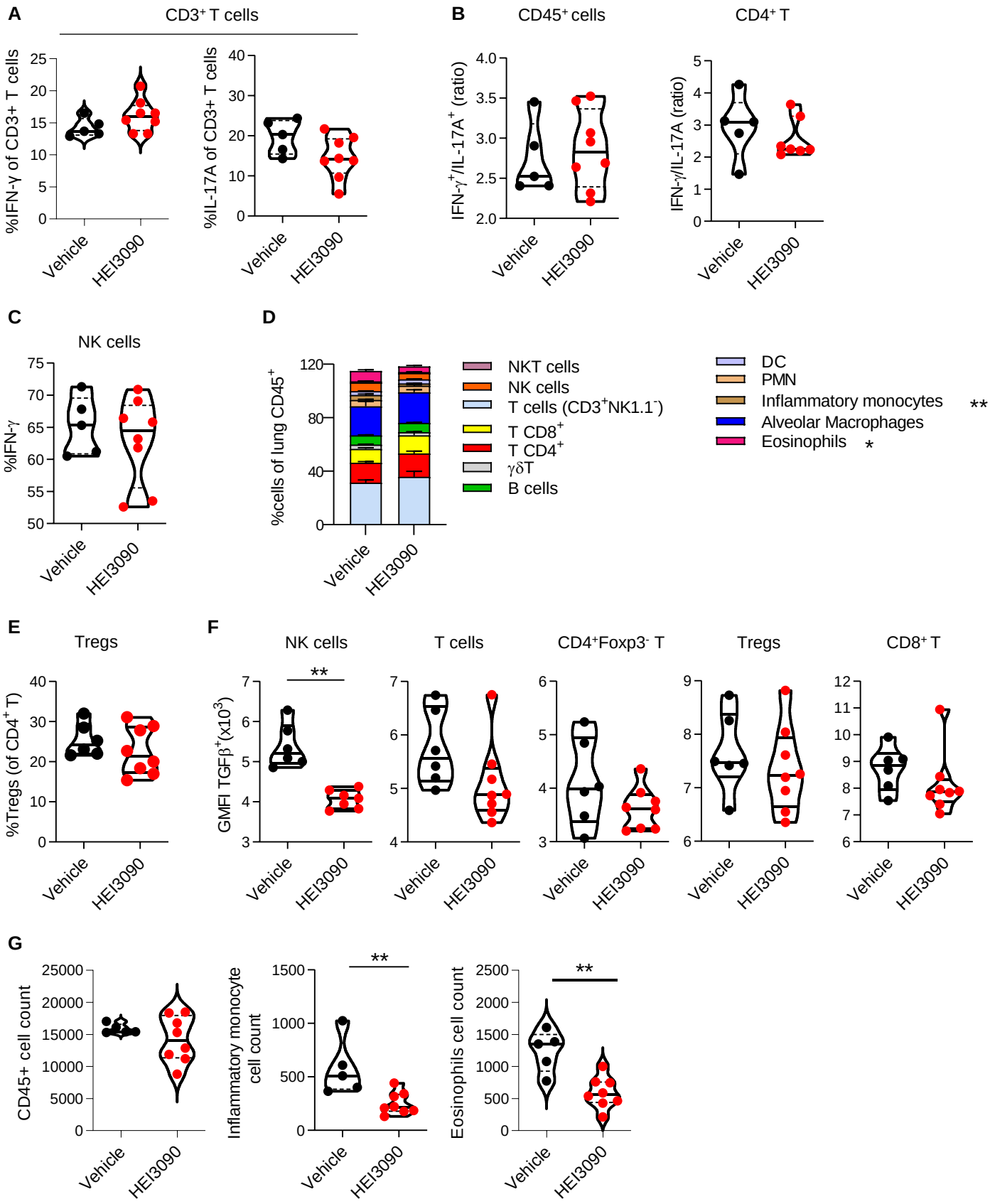
A
CD3+ T cells
%IFN-γ of CD3+ T cells
%IL-17A of CD3+ T cells
Vehicle
HEI3090
B
CD45+ cells
CD4+ T
IFN-γ+/IL-17A+ (ratio)
IFN-γ/IL-17A (ratio)
C
NK cells
%IFN-γ
D
%cells of lung CD45+
NKT cells
NK cells
T cells (CD3+NK1.1-)
T CD8+
T CD4+
γδT
B cells
DC
PMN
Inflammatory monocytes **
Alveolar Macrophages
Eosinophils *
E
Tregs
%Tregs (of CD4+ T)
F
NK cells
T cells
CD4+Foxp3- T
Tregs
CD8+ T
GMFI TGFβ+(x10^3)
**
G
CD45+ cell count
Inflammatory monocyte cell count
Eosinophils cell count

Supplemental Figure 3: Activation of P2RX7 with HEI3090 reshapes immune infiltration in the lungs

WT mice were given 2.5 U/kg at day 1 i.n. and treated for 14 days with 1.5 mg/kg of HEI3090 or Vehicle. At Day 14 lungs were analyzed by flow cytometry. **(A)** Percentage of IFN-γ producing and IL17A of TCD3 cells (CD45+CD3+). P-values were determined by Two-tailed unpaired t-test. **(B)** Ratio of IFN-γ over IL-17A in lung immune cells ($CD45^+$) or $CD4^+$T cells of WT mice. P-values were determined by Two-tailed unpaired t-test. **(C)** Percentage of IFN-γ producing NK cells ($NK1.1^+CD3^-$). P-values were determined by Two-tailed unpaired t-test. **(D)** Percentage of cells in lungs of mice. P-values were determined by two-way ANOVA with Tukey multiple comparisons test. Colored bars (mean + SEM) illustrate indicated cell populations. **(E)** Percentage of Tregs ($CD3^+CD4^+Foxp3^+NK1.1^-$) of $CD4^+$T cells. P-values were determined by Two-tailed unpaired t-test **(F)** GMFI of TGFβ+ NK cells, p-values were determined by Two-tailed unpaired t-test **(G)** CD45+, inflammatory monocytes and eosinophils cell count assessed by flow cytometry. P-values were determined by Two-tailed Mann-Whitney test. The violin plot illustrates the distribution of Ashcroft scores across indicated groups. The width of the violin at each point represents the density of data, and the central line indicates the median expression level. Each point represents one biological replicate. $*p < 0.05$, $**p < 0.01$. GMFI: geometric mean fluorescence intensity, Tregs: regulatory T cells, NK: Natural Killer, NKT: Natural Killer T cells, DC: Dendritic cells, PMN: polymorphonuclear cells.

Supp Fig4

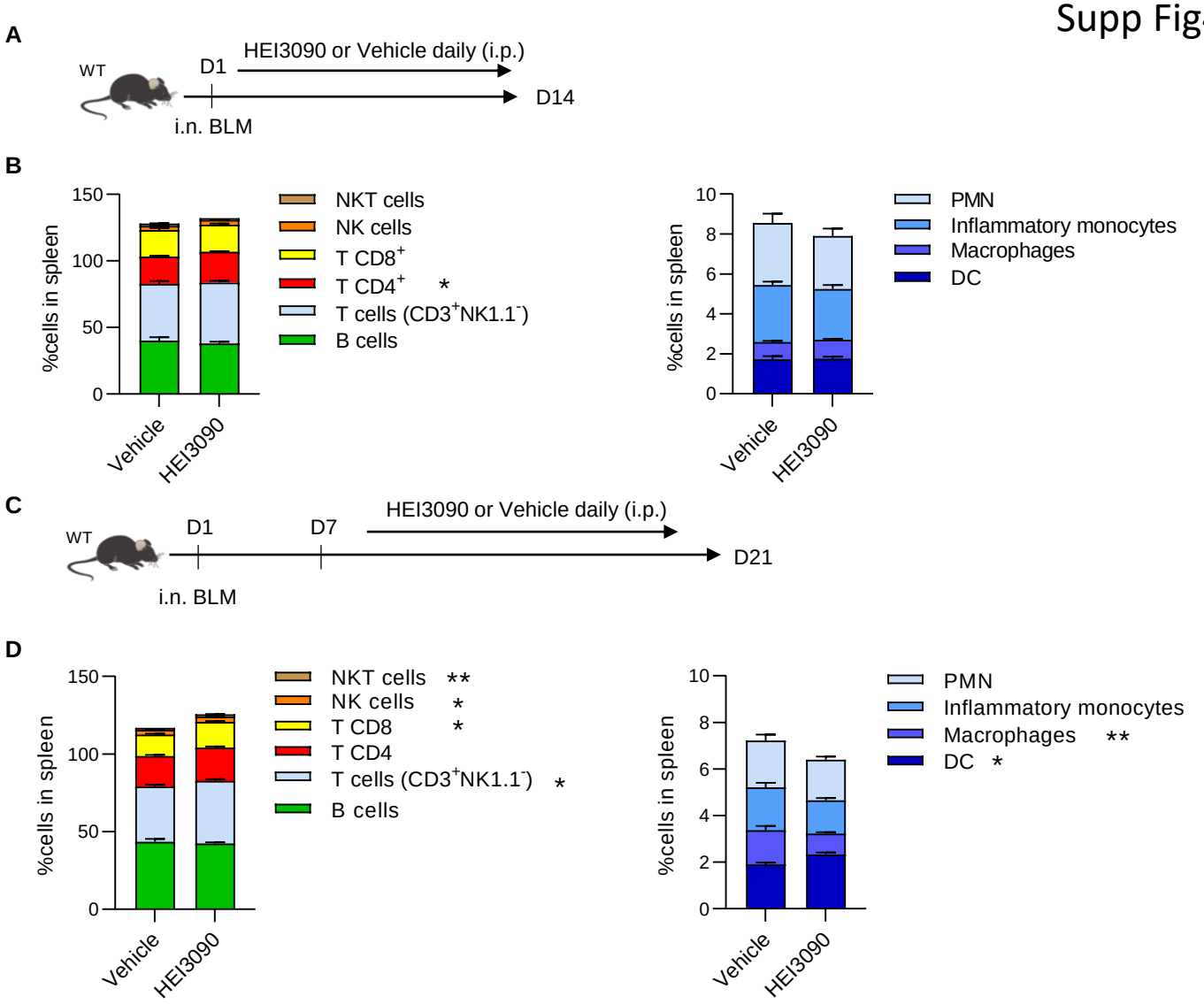

Supplemental Figure 4 : HEI3090 reactivates an immune response

(A) Experimental design. WT mice were given 2.5 U/kg at day 1 i.n. and treated for 14 days with 1.5 mg/kg of HEI3090 or Vehicle. **(B)** Percentage of immune cells of CD45+ in spleen assessed by flow cytometry at day 14. Percentage of cells in lungs of mice. . P-values were determined by two-way ANOVA with Tukey multiple comparisons test. Colored bars (mean + SEM) illustrate indicated cell populations. **(C)** WT mice were given 2.5 U/kg of bleomycin by i.n. route. 1.5 mg/kg of HEI3090 or vehicle were given daily 7 days after BLM administration until day 21. **(D)** Percentage of immune cells of CD45+ in spleen assessed by flow cytometry at day 21. Percentage of cells in lungs of mice. P-values were determined two-way ANOVA with Tukey multiple comparisons test. Colored bars (mean + SEM) illustrate indicated cell populations. Vehicle n = 13, HEI3090 n = 14. *$p < 0.05$, **$p < 0.01$. WT: Wildtype, BLM: bleomycin, i.p.: intraperitoneal, i.n.: intranasal, NK: Natural Killer, NKT: Natural Killer T cells, DC: Dendritic cells, PMN: polymorphonuclear cells.

Supp Fig5

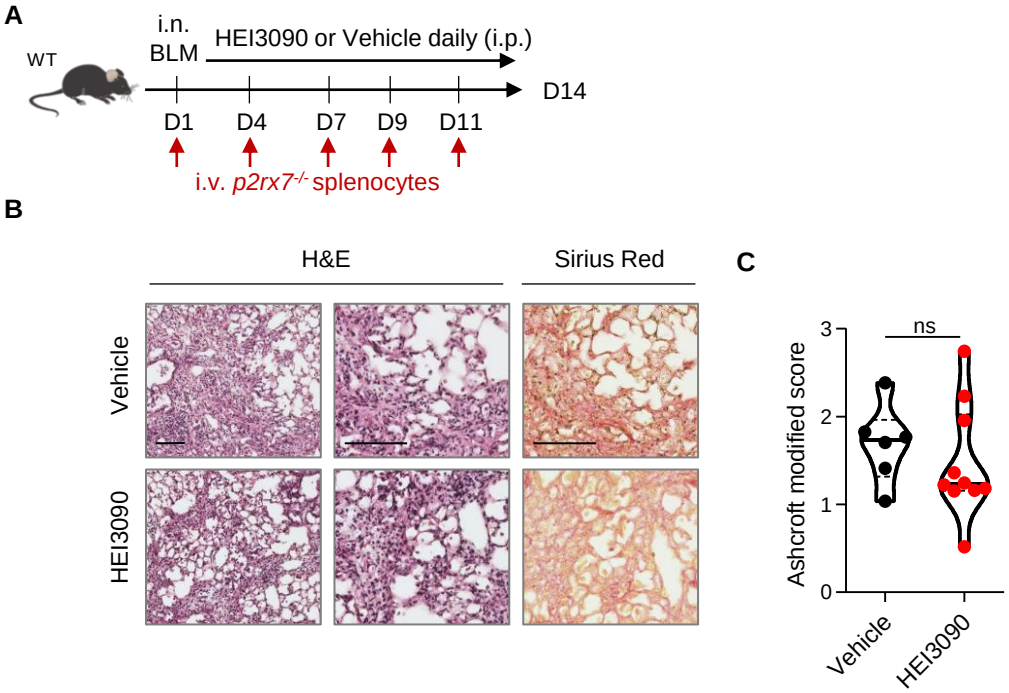

Supplemental Figure 5 : HEI3090 activity requires P2RX7's expressing immune cells.

(A) Experimental design. WT mice were given 2.5 U/kg of bleomycin by i.n. route and treated daily i.p. with 1.5 mg/kg of HEI3090 or Vehicle. Mice were given i.v. 3.10^6 *p2rx7*$^{-/-}$ splenocytes from male age-matched mice at day 1,4,7,9 and 11. **(B)** Representative images of lung sections at day 14 after treatment stained with H&E and Sirius Red, scale bar= 100 µm. **(C)** Fibrosis score assessed by the Ashcroft method. P-values were determined by Two-tailed unpaired t-test. The violin plot illustrates the distribution of Ashcroft scores across indicated groups. The width of the violin at each point represents the density of data, and the central line indicates the median expression level. Each point represents one biological replicate. ns, not significant.

Supp Fig6

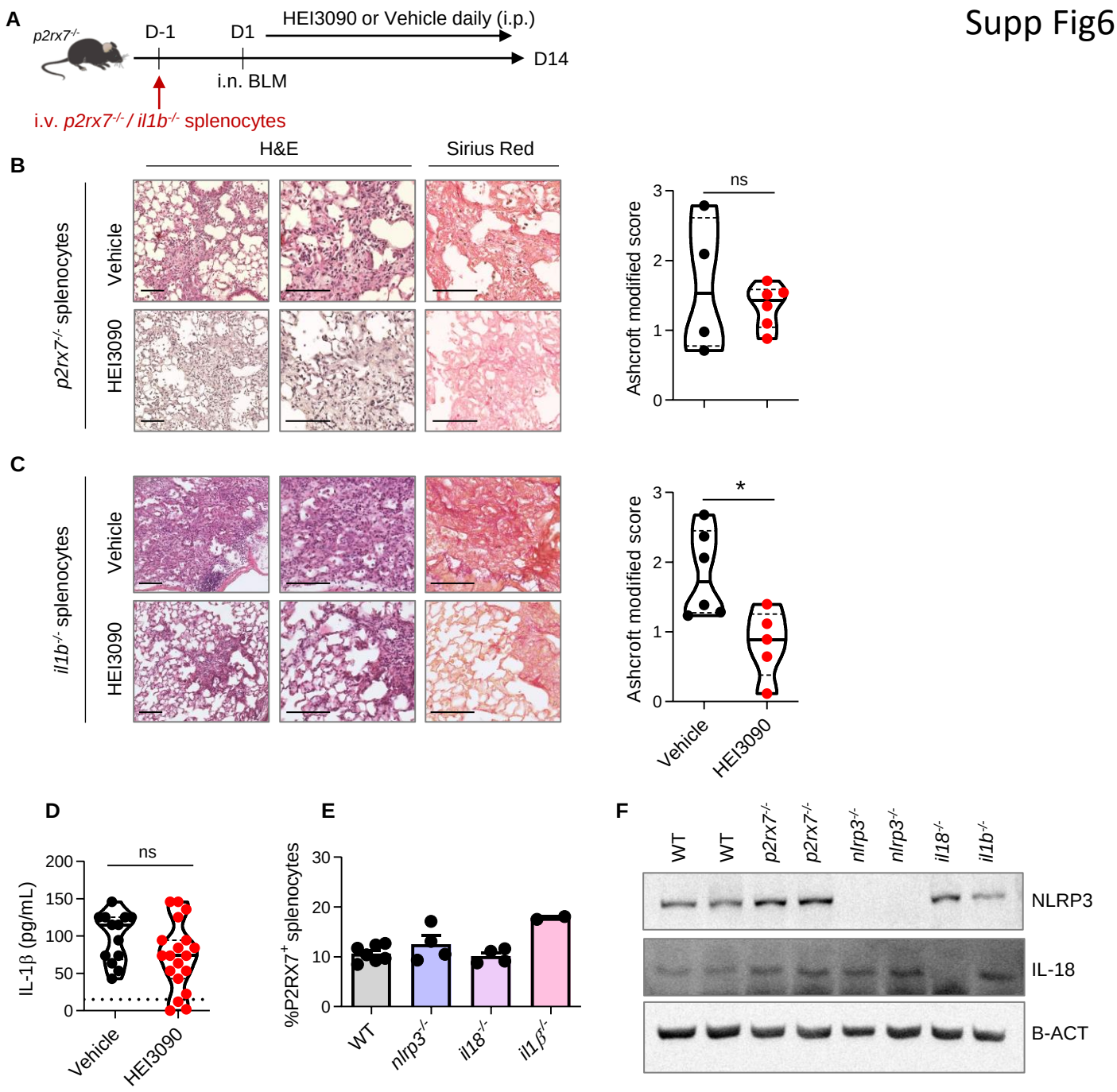

Supplemental Figure 7 : The antifibrotic effect of HEI3090 is independent of IL1B expression.

(A) Experimental design. *p2rx7*$^{-/-}$ mice were given 3.10^{6} *p2rx7*$^{-/-}$ or *il1β*$^{-/-}$ splenocytes i.v. one day prior to BLM delivery (i.n. 2.5 U/kg). Mice were treated daily i.p. with 1.5 mg/kg HEI3090 or vehicle for 14 days. **(B)** Representative images of lung sections at day 14 after treatment stained with H&E and Sirius Red with *p2rx7*$^{-/-}$ splenocytes, scale bar= 100 µm (left) and fibrosis score assessed by the Ashcroft method (right). P-values were determined by Two-tailed unpaired t-test **(C)** Representative images of lung sections at day 14 after treatment stained with H&E and Sirius Red with *il1β*$^{-/-}$ splenocytes, bar= 100 µm (left) and fibrosis score assessed by the Ashcroft method (right). P-values were determined by Two-tailed unpaired t-test **(D)** IL-1β levels in sera of WT mice at day 14 after treatment. P-values were determined by Two-tailed unpaired t-test **(E)** Percentage of P2RX7^{+} cells in spleens of WT and various KO mice assessed by flow cytometry. P-values were determined by one-way ANOVO, with Kruskal-Wallis test for multiple comparisons. Bar mean with SEM is showed. **(F)** NLRP3 and IL-18 expression in spleens of WT and various KO mice assessed by Western Blot. The violin plot illustrates the distribution of Ashcroft scores across indicated groups. The width of the violin at each point represents the density of data, and the central line indicates the median expression level. In all figures, each point represents one biological replicate. *$p < 0.05$. WT: Wildtype, BLM: bleomycin, i.p.: intraperitoneal, i.n.: intranasal, i.v.: intravenous, H&E: hematoxylin&eosin, KO: knock-out

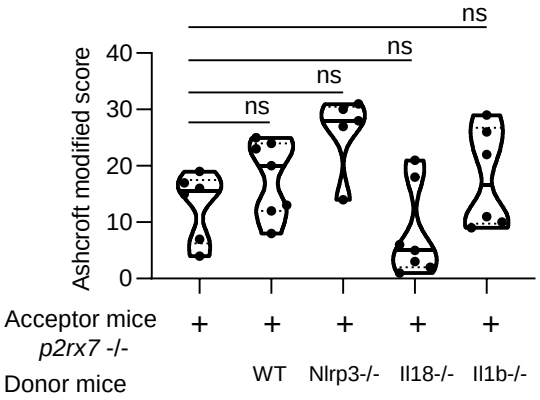

Supplemental Figure 7 : The genetic background does not impact lung fibrosis at steady step levels

p2rx7-/- mice were given 3.106 WT, nlrp3-/-, il18-/- or il1b -/- splenocytes i.v. one day prior to BLM delivery (i.n. 2.5 U/kg). p2rx7-/- mice or p2rx7-/- mice adoptively transferred with splenocytes from indicated genetic background were treated daily i.p. with 1.5 mg/kg HEI3090 or vehicle for 14 days. Fibrosis score assessed by the Ashcroft method. P-values were analyzed on all treated and non treated groups by one-way ANOVA, with Kruskal-Wallis test for multiple comparisons. The violin plot illustrates the distribution of Ashcroft scores across indicated experimental groups. The width of the violin at each point represents the density of data, and the central line indicates the median expression level. Each point represents one biological replicate. ns, not significant.

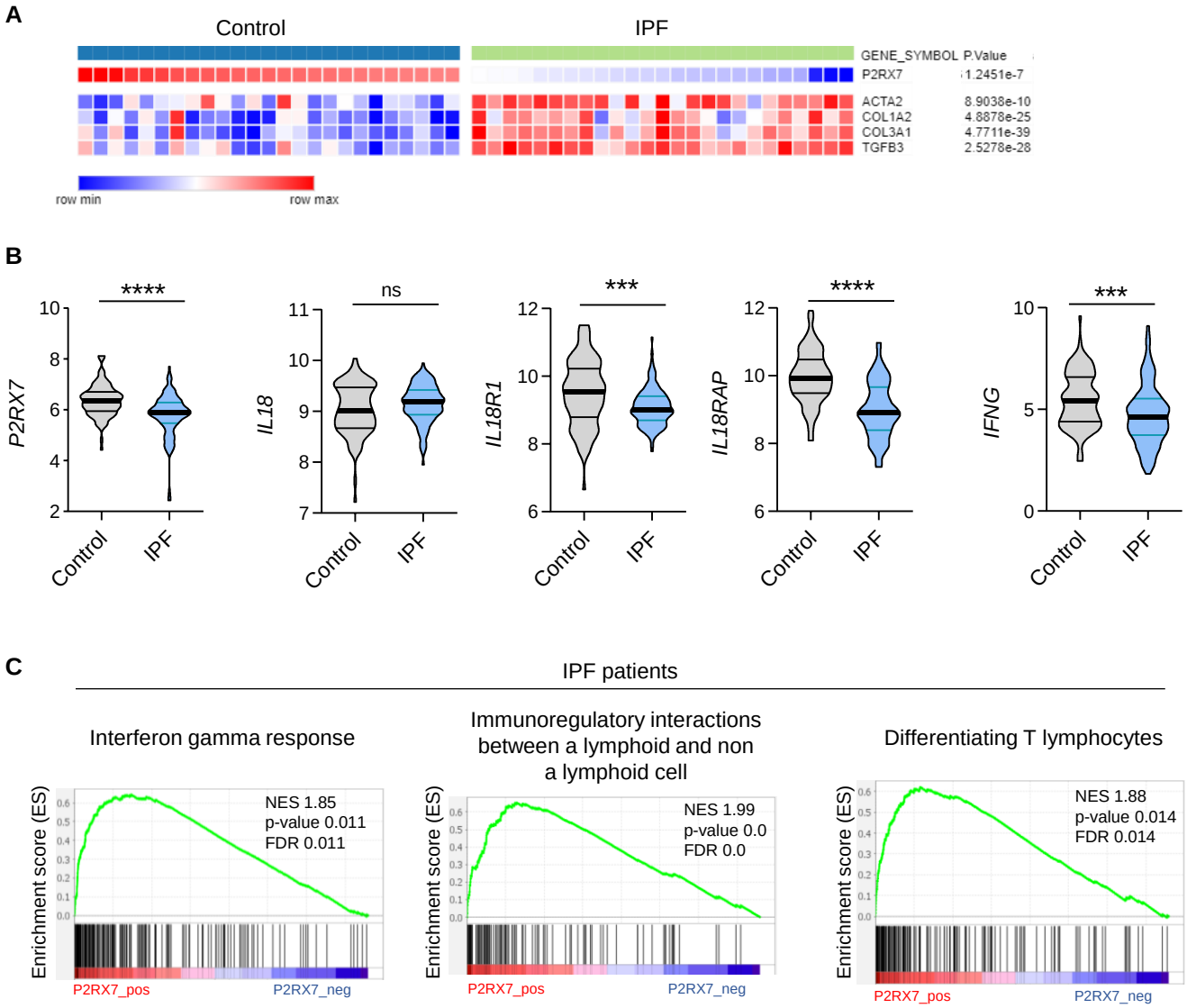

Figure 1 : The P2RX7/IL-18/IFN-γ pathway is downregulated in IPF

(A) Heatmap of mRNA expression of P2RX7 in control and IPF patients with a cluster of fibrosis-associated genes. Raw p-values are shown (Limma). P-values were determined by Spearman test. **(B)** mRNA expression of P2RX7, IL18, IL18R1, IL18RAP and IFNG between control and IPF patients from 213 individuals, corresponding to 91 controls and 122 IPF patients. P-values were determined by Two-tailed unpaired t-test or Mann-Whitney t-test. ***$p < 0.001$, ****$p < 0.0001$. **(C)** Gene set enrichment analysis (GSEA) plot associating P2RX7 mRNA levels from IPF patients with three immunological signatures. The green line represents the enrichment score and the black lines the specific signature-associated genes. NES: Normalized enrichment score, p-values (bilateral Kolmogorov–Smirnov), and false discovery rate (FDR) are shown.

Fig2

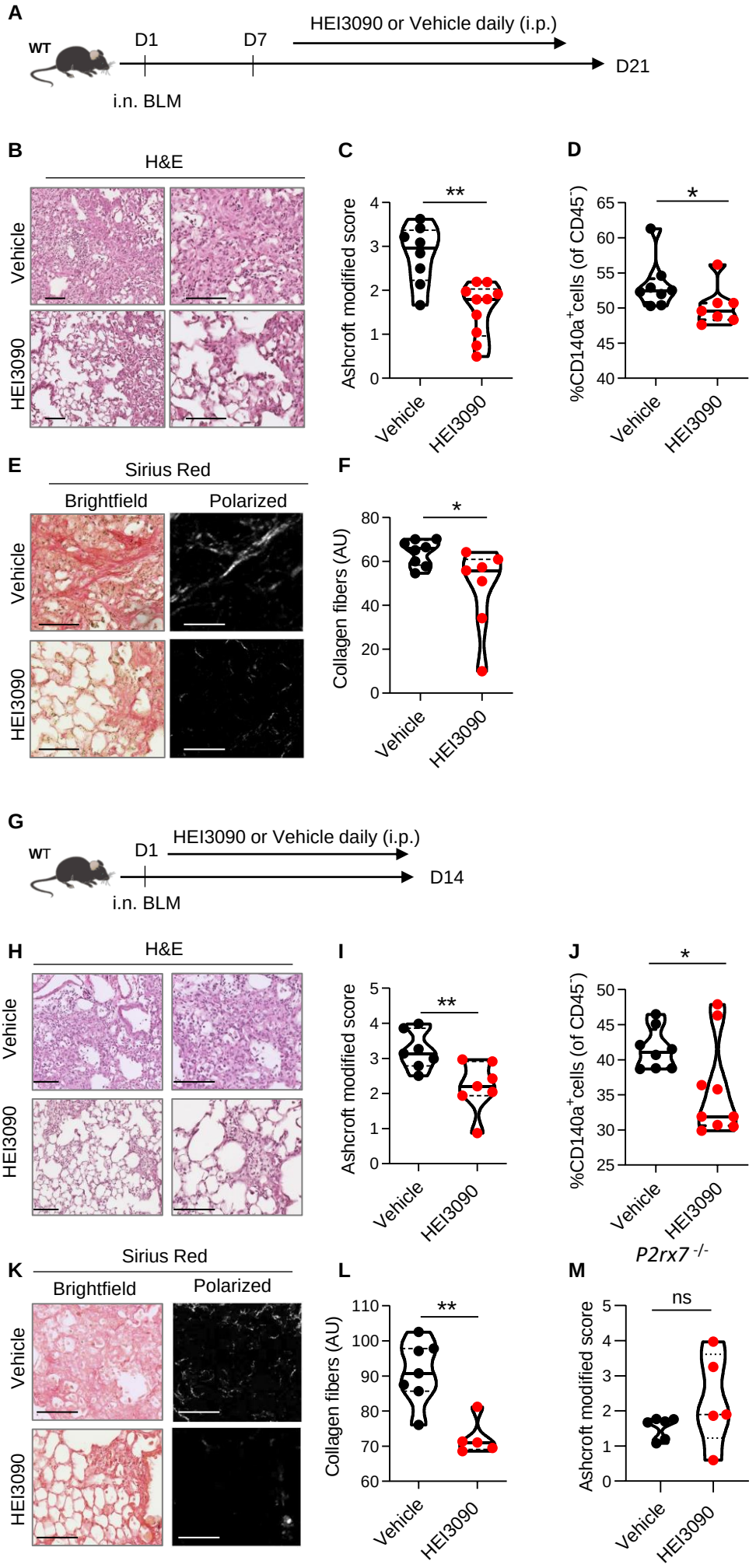
A
WT
D1
D7
HEI3090 or Vehicle daily (i.p.)
D21
i.n. BLM
B
H&E
Vehicle
HEI3090
C
Ashcroft modified score
**
Vehicle
HEI3090
D
%CD140a+cells (of CD45-)
*
Vehicle
HEI3090
E
Sirius Red
Brightfield
Polarized
Vehicle
HEI3090
F
Collagen fibers (AU)
*
Vehicle
HEI3090
G
WT
D1
HEI3090 or Vehicle daily (i.p.)
D14
i.n. BLM
H
H&E
Vehicle
HEI3090
I
Ashcroft modified score
**
Vehicle
HEI3090
J
%CD140a+cells (of CD45-)
*
Vehicle
HEI3090
P2rx7 -/-
K
Sirius Red
Brightfield
Polarized
Vehicle
HEI3090
L
Collagen fibers (AU)
**
Vehicle
HEI3090
M
Ashcroft modified score
ns
Vehicle
HEI3090

Figure 2 : HEI3090 attenuates lung fibrosis progression

(A) Experimental design. WT mice were given 2.5 U/kg of bleomycin by i.n. route. At the end of the inflammatory phase (d7), 1.5 mg/kg of HEI3090 or vehicle were given daily until day 21. (**B)** Representative images of lung sections at day 21 after treatment stained with H&E and Sirius Red, Scale bar= 100 µm. **(C)** Fibrosis score assessed by the Ashcroft method. P-values were determined by Two-tailed unpaired t-test. **(D)** Quantification of fibroblasts/myofibroblasts in non-immune cell subset. P-values were determined by Two-tailed Mann-Whitney test. **(E)** Representative images of lung sections at day 21 after treatment stained with Sirius Red, Scale bar= 100 µm. **(F)** Collagen levels in whole lung of mice assessed on Sirius Red-polarized images. P-values were determined by Two-tailed unpaired t-test. **(G)** Experimental design. WT mice were given 2.5 U/kg of bleomycin by i.n. route. 1.5 mg/kg of HEI3090 or vehicle were given daily until day 14. **(H)** Representative images of lung sections at day 14 after treatment stained with H&E, Scale bar= 100 µm. **(I)** Fibrosis score assessed by the Ashcroft method. P-values were determined by Two-tailed unpaired t-test. **(J)** Quantification of fibroblasts/myofibroblasts in non-immune cell subset. P-values were determined by Two-tailed Mann-Whitney test. **(K)** Representative images of lung sections at day 14 after treatment stained with Sirius Red, Scale bar= 100 µm. **(L)** Collagen levels in whole lung of mice assessed on Sirius Red-polarized images. P-values were determined by Two-tailed Mann-Whitney test. **(M)** P2rx7 KO mice were given 2.5 U/kg of bleomycin by i.n. route. 1.5 mg/kg of HEI3090 or vehicle were given daily until day 14. Fibrosis score assessed by the Ashcroft method is showed. P-values were determined by Two-tailed Mann-Whitney test. For all analyses, the violin plot illustrates the distribution of Ashcroft scores across indicated groups. The width of the violin at each point represents the density of data, and the central line indicates the median expression level. Each point represents one biological replicate. $*p < 0.05$, $**p < 0.01$. WT: Wildtype, BLM: bleomycin, i.p.: intraperitoneal, i.n.: intranasal, H&E: hematoxylin & eosin, AU: arbitrary units.

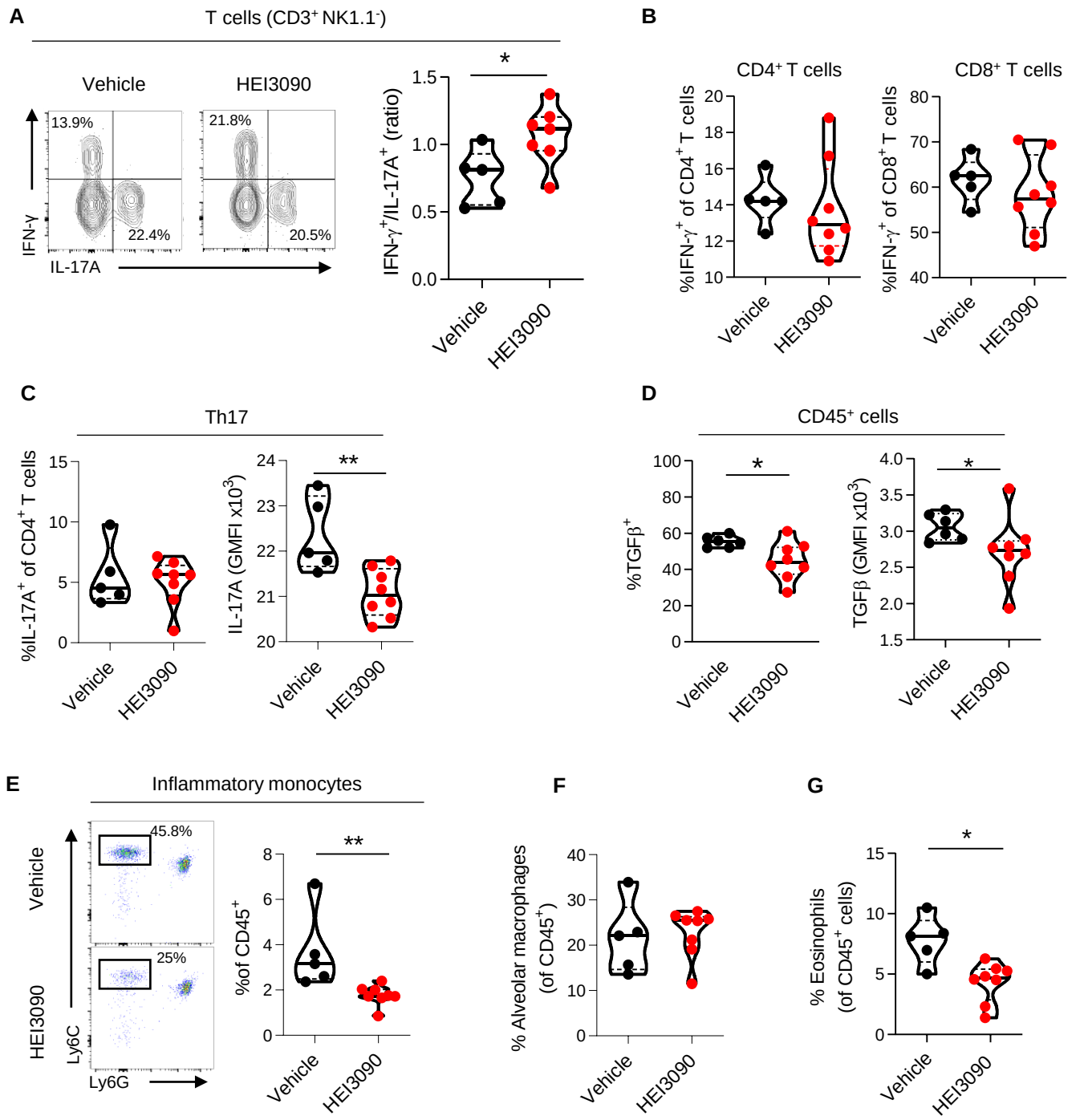

Figure 3 : HEI3090 favors an anti-fibrotic immune signature in the lungs

WT mice were given 2.5 U/kg of bleomycin by i.n. route and treated daily i.p. with 1.5 mg/kg of HEI3090 or Vehicle. Lungs were analyzed by flow cytometry at day 14. **(A)** Contour plot of IFN-γ and IL-17A producing T cells (CD3+NK1.1-) (left) and ratio of IFN-γ over IL-17A in T cells (CD3+NK1.1-) (right). P-values were determined by Two-tailed Mann-Whitney test. **(B)** Percentage of IFN-γ producing CD4+ and CD8+ T cells. P-values were determined by Two-tailed Mann-Whitney test. **(C)** Percentage and GMFI of IL-17A+ cells of CD4+ T cells (CD3+CD4+NK1.1-). P-values were determined by Two-tailed Mann-Whitney test. **(D)** Percentage and GMFI of TGFβ in CD45+ cells. P-values were determined by Two-tailed Mann-Whitney test. **(E)** Dotplot showing lung inflammatory monocytes, gated on lineage-CD11c-CD11b+ cells (left) and percentage of lung inflammatory monocytes (Ly6ChighLy6G-) (right). P-values were determined by Two-tailed Mann-Whitney test. **(F)** Percentage of alveolar macrophages (CD11c+SiglecF+), p-values were determined by Two-tailed unpaired t-test and **(G)** lung eosinophils (CD11b+SiglecF+CD11c-), p-values were determined by Two-tailed Mann-Whitney test. **(A-G),** The violin plot illustrates the distribution of Ashcroft scores across indicated groups. The width of the violin at each point represents the density of data, and the central line indicates the median expression level. Each point represents one biological replicate. *$p < 0.05$, **$p < 0.01$. GMFI: geometric mean fluorescence intensity. i.n.: intranasal, i.p.: intraperitoneal.

Fig4

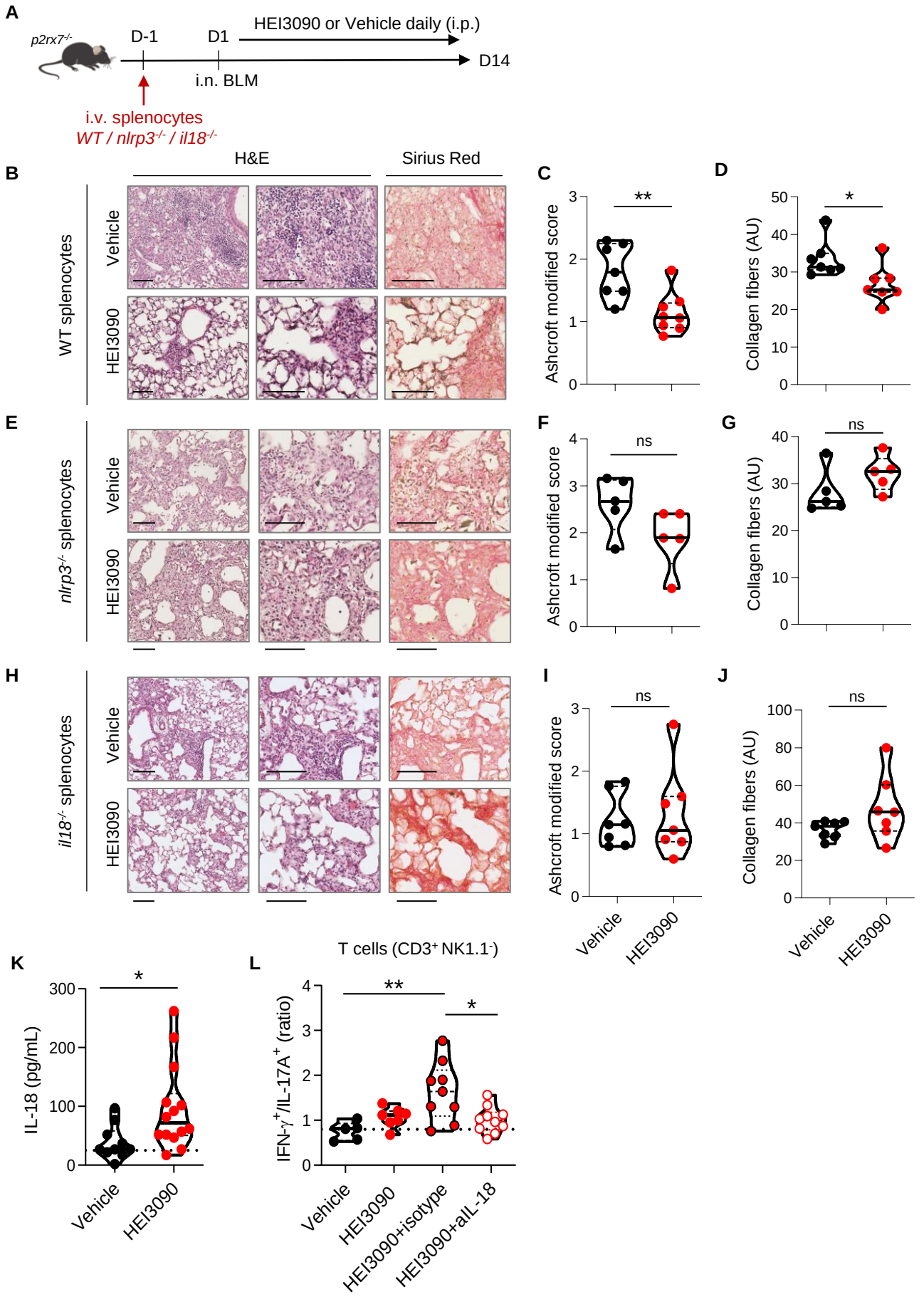
A
p2rx7-/-
D-1
D1
HEI3090 or Vehicle daily (i.p.)
D14
i.n. BLM
i.v. splenocytes
WT / nlrp3-/- / il18-/-
B
H&E
Sirius Red
WT splenocytes
Vehicle
HEI3090
C
Ashcroft modified score
**
D
Collagen fibers (AU)
*
E
nlrp3-/- splenocytes
F
ns
G
H
il18-/- splenocytes
I
J
Vehicle
HEI3090
K
IL-18 (pg/mL)
L
T cells (CD3+ NK1.1-)
IFN-γ+/IL-17A+ (ratio)
HEI3090+isotype
HEI3090+aIL-18

Figure 4: The P2RX7/NLRP3/IL-18 pathway in immune cells is required for HEI3090's antifibrotic effect

(A) Experimental design. p2rx7-/- mice were given 3.106 WT, nlrp3-/- or il18-/- splenocytes i.v. one day prior to BLM delivery (i.n. 2.5 U/kg). Mice were treated daily i.p. with 1.5 mg/kg HEI3090 or vehicle for 14 days. **(B,E,H)** Representative images of lung sections at day 14 after treatment stained with H&E and Sirius Red, scale bar= 100 µm. **(C, F, I)** Fibrosis score assessed by the Ashcroft method and **(D, G, J)** Collagen fiber intensity. **(C)** WT splenocytes, p-values were determined by Two-tailed Mann-Whitney test. **(D)** WT splenocytes, p-values were determined by Two-tailed unpaired t-test. **(F, G)** nlrp3-/- splenocytes, p-values were determined by Two-tailed Mann-Whitney test. **(I, J)** il18-/- splenocytes, p-values were determined by Two-tailed Mann-Whitney test. **(K)** IL-18 levels in sera of WT BLM-induced mice at day 14. P-values were determined by Two-tailed unpaired t-test. **(L)** Ratio of IFN-γ over IL-17A in lung T cells (CD3+NK1.1-) of WT mice neutralized for IL-18 or not (isotype control) every 3 days. P-values were determined by one-way ANOVA with Tukey's multiple comparisons test. For all analyses, the violin plot illustrates the distribution of Ashcroft scores across indicated groups. The width of the violin at each point represents the density of data, and the central line indicates the median expression level. Each point represents one biological replicate. *$p < 0.05$, **$p < 0.01$ WT: Wildtype, BLM: bleomycin, i.p.: intraperitoneal, i.n.: intranasal, i.v.: intravenous, H&E: hematoxylin & eosin.